Combustion and Flame 247 (2023) 112498

Contents lists available at ScienceDirect

Combustion and Flame

journal homepage: www.elsevier.com/locate/combustflame

Reaction kinetics for high pressure hydrogen oxy-combustion in the presence of high levels of H_2O and CO_2

Ashkan Beigzadeh[a,c,*], Mohammed Alabbad[b,*], Dapeng Liu[b], Khalid Aljohani[b], Khaiyom Hakimov[b], Touqeer Anwar Kashif[b], Kourosh Zanganeh[a], Eric Croiset[c], Aamir Farooq[b]

[a] Natural Resources Canada (NRCan), CanmetENERGY-Ottawa (CE-O), 1 Haanel Dr., Ottawa, ON K1A 1M1, Canada
[b] King Abdullah University of Science and Technology, Clean Combustion Research Center, Physical Science and Engineering Division, Thuwal 23955-6900, Saudi Arabia
[c] Department of Chemical Engineering, University of Waterloo, 200 University Avenue West, Waterloo, ON N2L 3G1, Canada

ARTICLE INFO

Article history:
Received 24 August 2021
Revised 4 November 2022
Accepted 4 November 2022
Available online 23 November 2022

Keywords:
Hydrogen
Syngas
Kinetic mechanism
Ignition delay time
Pressurized oxy-fuel

ABSTRACT

Novel shock tube experimental ignition delay time (IDT) data are provided to delineate the impact of high concentrations (45% by mole) of H_2O and CO_2 on IDTs of stoichiometric 4% H_2. Ignition delay experiments were conducted using a high- and a low-pressure shock tube facility. High-pressure experiments were performed at pressures of 37-43.8 bar and temperatures of 1084-1242 K in four different bath gases, namely: Ar, 45%H_2O/Ar, 30%H_2O/15%CO_2/Ar, and 45%CO_2/Ar. Low-pressure experiments were conducted at 2.1-2.7 bar and 926-1198 K in Ar and 45%CO_2/Ar bath gases. Impacts of non-ideal ignition phenomena that may occur in the presence of large amounts of H_2O and CO_2 were also analyzed. A minimally-tuned H_2/CO reaction mechanism, CanMECH 1.0, targeting high-pressure combustion in the presence of large concentrations of H_2O and CO_2 is presented. The mechanism is constructed from unadjusted kinetic rate parameters from theoretical / experimental elementary reaction rate determinations. The only adjusted rate in CanMECH 1.0 is the much disputed Ar-specific low-pressure-limit pre-exponential factor of $H + O_2 (+Ar) = HO_2 (+Ar)$ within the uncertainty bounds of the source rate. Validity of CanMECH 1.0 is confirmed against shock tube IDT data of this work, as well as selected H_2 and H_2/CO shock tube IDT datasets from literature. The performance of the model is compared to Keromnes et al. model (Combust. Flame 160 (2013) 995-1011). CanMECH 1.0 outperformed Keromnes et al. for 16 datasets out of 26 and exhibited a similar performance for another two. In particular, CanMECH 1.0 outperformed Keromnes et al. in predicting shock tube IDTs for H_2O- and CO_2-laden reactive mixtures, as well as all IDT data at pressures of 17-43.8 bar, which are of distinct value to pressurized oxy-fuel combustion applications relevant to this work.

1. Introduction

It is expected that global energy demand will grow by 4-9% for the period of 2019-2030, and that natural gas (NG) demand will increase by 30% in the next two decades [1]. Continued use of NG necessitates demonstrable progress in technologies like carbon capture, utilization and storage (CCUS) [1]. As one promising carbon capture pathway, oxy-fuel combustion entails reacting the fuel with pure oxygen, producing a flue gas composed mostly of CO_2 and H_2O, from which CO_2 can be easily separated [2]. To improve the economics of CCUS, "transformative" highly-pressurized oxy-fuel systems are under development [3–5]. To unearth the true potential of these technologies, knowledge gaps associated with their combustion chemistry need to be addressed.

The body of research is growing for direct pressurized oxy-fuel combustion chemistry [6–10], but not for indirect cycles' [4]. From a chemical kinetics standpoint, one main difference is higher H_2O concentrations, upwards of 65 mole%, for indirect cycles vs. high CO_2 concentrations in direct cycles [3,4]. Studies have evaluated the effect of small moisture addition to gas turbine inlets for improved combustion performance and emissions control [11,12]. Mazas et al. [11] investigated the effects of CO_2 and H_2O addition on premixed oxy-methane laminar flame speeds in CO_2

* Corresponding authors.
E-mail addresses: ashkan.beigzadeh@NRCan-RNCan.gc.ca (A. Beigzadeh), mohammed.abbad@kaust.edu.sa (M. Alabbad).

https://doi.org/10.1016/j.combustflame.2022.112498

and N_2, with small steam concentrations. They observed a quasi-linear decrease in flame speed with increased H_2O and CO_2 dilution [11]. Donohoe et al. [12] investigated the effect of small steam dilution rates on ignition of H_2, syngas and NG blends in Ar, and noted that significant changes in the thermal properties of the mixtures affect the overall reactivity. Turanyi et al. [13] noted the influence of bath gases on H_2O_2 decomposition; they stated that species that have similar molecular energy levels to the rovibrationally excited H_2O_2 molecules, like H_2O_2 and H_2O, have larger collision efficiencies, whereas noble gases have typically small collision efficiencies. Klippenstein [14] reviewed the rate of $H+O_2(+M)=HO_2(+M)$ and concluded that it is important to evaluate this reaction with H_2O as a collider, as a key contributor to HO_2 stabilization. Baulch et al. [15] noted that there are few measurements that specifically address third-body efficiency factors, which can be quite uncertain and temperature dependent [15], and that this lack of data hinders even an approximate parameterization. Shao et al. [16] conducted shock tube ignition delay time (IDT) experiments of stoichiometric 3%H_2 with 3.9-13.8%H_2O/Ar at ~15 bar and 1264-1376 K and confirmed that the relative collision efficiency of H_2O to Ar is 23. This is in contrast to Klippenstein's speculation that the impact of H_2O may be lower than perceived [14].

This work reports novel sets of shock tube IDT experimental data involving mixtures of 4%H_2 at an equivalence ratio (φ) of 1 with 0-45%H_2O/Ar and 0-45%CO_2/Ar and pressures near 2 and 40 bar absolute. Additionally, it provides an H_2/CO oxidation mechanism, targeting pressurized oxy-combustion kinetics in the presence of large concentrations of H_2O and CO_2, validated against a select number of shock tube ignition delay time experimental datasets.

2. Numerical modeling approach

The shock tube IDT modeling approach aims to reproduce the experimentally measured pressure and OH* emission trends preceding ignition. For IDT experiments, it is imperative to accurately model the reactor from the time the reflected shockwave arrives at the observation location to the runaway increase in OH* emission, signifying ignition. The shock tube is modelled as a constrained volume reactor because of measured pressure spikes at ignition, see supplementary Fig. S1. The transient energy equation is solved to track the evolution of species and reactor conditions. Auto-ignition simulations were conducted in Chemkin-Pro [17] using its 0D homogeneous adiabatic batch reactor model with no wall effects. Additionally, it is important to accurately model the gradual pressure-rise behind reflected shock wave, known as the dp/dt effect, which affects the temperature. Due to the short duration (smaller than 2 ms) ignition delays reported here, sensitivity analyses confirmed that the modelled ignition delay times were not very sensitive to small variations in dp/dt values. Moreover, as relatively larger pressure noise is associated with pressure traces of H_2O- and CO_2-diluted bath gases, in lieu of measured experiment-specific pressure profile, facility-specific average dp/dt was converted in this work to a mixture-specific volume profile and input as dv/dt profile in Chemkin-Pro [17], assuming isentropic compression.

For thermodynamic properties, Burke et al. [18] at National University of Ireland Galway (NUIG) recently conducted a comprehensive review of the literature including thermochemical properties from NIST [19] and ATcT [20] databases among others, and assembled a database of thermochemical properties [18]. In this study, NUIG's updated temperature-dependent thermochemical properties, from their well-cited AramcoMech3.0 mechanism [21], are adopted for IDT simulations.

NIST provides thermophysical properties as a function of pressure for some species [19]. These properties are used in this work to estimate the error introduced by the assumption of pressure-independency of the temperature-dependent properties. To estimate the errors of post-reflected shock reactor temperatures (T_5) and pressure (P_5), NIST's pressure-dependent properties were compared with Burcat and Ruscic's [22] pressure-independent properties. These errors, while within the reported uncertainty bounds of Burcat and Ruscic's [22] at low pressures, were re-evaluated for the high-pressure experiments involving large concentrations of H_2O and CO_2. Comparison of H_2O and CO_2 C_Ps from Burcat and Ruscic's [22] vs. NIST REFPROP's [19] reveals the former underpredicts them for both post-incident and -reflected shock conditions of 40 bar experiments. In this work, H_2O and CO_2 C_p's positive error bars were adjusted to +1.8% and 0.63%, respectively, for uncertainty calculations.

Pressure-dependent reactions are an important feature of this work due to combined effects of high pressure and large concentrations of H_2O and CO_2. To detect whether a reaction could be pressure-dependent, an automatic reaction mechanism generator software, called RMG [23], was used which constructs reaction networks and estimates phenomenological pressure-dependent rate coefficients using simplified RRKM-based calculations [23,24].

To effectively segregate and characterize the impact of strong and weak colliders, such as H_2O and Ar, on the kinetics, Troe's "multiple expression" formulation is used when possible. This enables implementing multiple collider-specific low-pressure-limit expressions and broadening factors, with a common high-pressure-limit rate. Earlier reported issues of overestimations of the rate, associated with multiple-expression treatment by Burke et al. [25], Burke and Song [26], and Konnov [27] are addressed by Chemkin-Pro's modified multiple-expression formulation and mixture rule.

In summary, as the targeted bath gases, containing large quantities of H_2O and CO_2, are significantly different from the traditionally explored Ar- or N_2-diluted mixtures, this work proposes a mechanism with minimal kinetic rate parameter adjustments. As the envisioned applications of these bath gases pertain to future combustors which operate at high pressures (100-300 bars), the model also includes a comprehensive set of pressure- and collider-specific kinetic rate parameters. These parameters can be utilized as adjustment levers to enable independent examination of the effects of pressure dependence, the temperature dependence of these pressure dependencies, as well as the impact of the collider efficiency. This paper aims to develop a kinetic mechanism which can serve as a platform for future rate parameter improvements targeting uncommon bath gases, such as H_2O and CO_2. To this end, this work prescribes the following step-wise model development and improvement methodology:

1) Examination of literature for careful selection of reaction rates obtained through elementary theoretical/experimental rate determination studies;
2) Implementation of pressure-dependent multiple-expression collider specific reaction rates of Troe type, in particular, for applications with varying collider efficiencies and temperature dependencies;
3) Selection of high-quality validation data, minimally impacted by non-ideal effects (e.g., impurities, shock bifurcation);
4) Propose/conduct studies targeted at improved elementary theoretical or experimental reaction rate determinations for key reactions, and when not feasible, raise awareness on gaps for such reaction rates;
5) After exhausting the above four steps, one can resort to limited parameter adjustments within the uncertainty bounds stip-

ulated by the source elementary reaction rate determination studies;

6) With the emergence of higher accuracy rate determinations for sensitive reactions, revert any previous parameter adjustments and repeat steps 3-5.

3. Experimental approach

Shock tube IDT experiments at pressures of 2 and 40 bar were carried out for H_2 oxidation. The experiments were designed to minimize the effect of impurities and non-ideal effects on IDTs, to achieve feasible IDT test times, to minimize the onset of pre-ignition, and to reduce reflected shock bifurcation effects by judiciously capping H_2O and CO_2 concentrations, as illustrated below.

Urzay et al. [28], Mulvihill and Petersen [29], and Ninnemann et al. [30] have shown that hydrogen IDT experiments can be highly impacted by the presence of impurities. Mulvihill and Petersen [29] showed impurity effects are improbable at dilution levels of less than 94%. Conversely, Pang et al. [31] and Ninnemann et al. [30] showed that IDT experiments with 15% hydrogen exhibit pre-ignition, whereas lower concentration of 4% H_2 is less prone to it. Hence, experiments were designed with a concentration of 4% H_2 in this work, and literature data with H_2 concentrations less than 3% and greater than 15% were not used for model validation.

Pyror et al. [7] showed that for IDTs at shorter time scales, the magnitude of uncertainties becomes unacceptably large, rendering them ineffective as validation targets. To design experiments with practical IDTs, simulations were performed using Keromnes et al.'s model [32], targeting IDTs larger than 100 µs and smaller than 2 ms. The latter limit precludes contact surface or expansion fan arrival effects on ignition at the test plane, as well as high sensitivities of simulated ignition delay times to potential deviations from the assumed facility-specific average dp/dt values coupled with the gas dynamic model.

Presence of large quantities of polyatomic gases results in the bifurcation of the reflected shock [33]. Petersen and Hanson [33] investigated the extent and magnitude of bifurcation, and found they were a strong function of specific heat ratio (γ) [33]. Their experiments spanned 11-265 atm and γ of 1.29-1.59 [33], and showed that high levels of bifurcation did not affect the core portion of the post-shock region, comprising most of the flow area. Hargis and Petersen [34] investigated the effect of N_2 and CO_2 with mixture γ of 1.31-1.39, and reported high measurement uncertainties for γ values of 1.31 and 1.33. Pryor et al. [7] investigated the impact of CO_2 dilutions of up to 89.5% on the homogeneity of CH_4 ignition, using shock tube end-wall high-speed imaging, and showed that flame area ratio dropped to 71% at CO_2 dilution of 60% [7].

In-line with the above conclusions [7,33], and based on Hargis and Petersen's [34] pressure and emission traces, γ values larger than 1.4 were targeted in this work which limited maximum H_2O and CO_2 concentrations to ~45% (see supplementary Table S1).

Another challenge associated with the presence of H_2O and CO_2 is their quenching effect on excited species, such as OH^*, which results in significantly weaker emission signals observed. H_2O is twice as effective as CO_2, and three orders of magnitude more effective than Ar in de-exciting OH^* to OH. This can be observed by comparing the rate constants of reactions $OH^*+H_2O=OH+H_2O$ and $OH^*+CO_2=OH+CO_2$ with $OH^*+Ar=OH+Ar$ (see Fig. S2). Amplification of photo multiplier emission detector signal, while helpful, increased the noise associated with this signal.

It is also important to examine the possibility of the formation of hot spots and their effect on global IDT determinations. To this end, two non-dimensional numbers, ignition Damköhler number (Da_{ig}) and bifurcation Damköhler number (Da_{bif}), were calculated herein [35,36]. The associated analyses and results are detailed in the supplementary material section 3.2.

The ignition Damköhler number Da_{ig}, introduced by Labastida et al. [35], compares the time scale of thermal diffusivity of an ignition kernel developed from a hot spot to that of global induction time. Da_{ig} was evaluated for the targeted experimental conditions of this work. For the majority of conditions explored herein, the ignition Damköhler number was much larger than 1, which implies heat diffusion from potential hot spots takes much longer than the global induction timescales. Similarly, the bifurcation Damköhler number (Da_{bif}) proposed by Gordon and Ihme [36], which compares the time scales of shock bifurcation with the total ignition time, was also determined for all IDT experiments of this work. Gordon and Ihme [36] introduced a limiting value of $Da_{bif} = 1$ above which only strong or homogeneous ignition is observed. Most of the IDT experiments reported here exhibit bifurcation Damköhler numbers larger than 1 (See Fig. S5). For some experiments of mixtures containing 45%H_2O and 30%H_2O/15%CO_2, Da_{bif} values of ~0.3 to 1 are obtained. Gordon and Ihme's [36] suggested limiting value relies heavily on the timescale at which the bifurcation height equals half of the shock tube radius (D/4). However, for mixtures with lower reactivity, larger bifurcation heights may need to be reached to impact the main ignition event. This was observed recently by Labastida et al. [35] for methane mixtures where a strong ignition was observed for experiments with Da_{bif} as low as 0.27. Therefore, for the low-reactivity mixtures of this work (94% dilution), it is expected that the main ignition events are minimally impacted by bifurcation effects. The combination of these two analyses suggests that the IDT results presented here are unlikely to be affected by thermal diffusion or bifurcation effects.

Another concern is the possibility of ignition happening away from the end-wall due to the attenuation of the incident shock. To confirm that the highest temperature leading to ignition does occur at locations nearest to the driven section end-wall, axial temperature profile in the shock tube driven section was modelled. Detailed analyses presented in the supplementary material section number 3.3 illustrate that while higher T_2 temperatures may be observed away from the end-wall due to the attenuation of the incident shock, the highest T_5 temperatures are shown to occur at locations closest to the driven section end-wall due to the attenuation of the reflected shock wave (See Fig. S8). Therefore, the experimental results presented in this work are not expected to be impacted by far-wall ignition effects.

4. Reaction mechanism

The H_2-O_2 mechanism proposed herein is intended to serve as sub-mechanism of a hierarchical hydrocarbon (HC) kinetics model, targeting oxy-fuel combustion conditions. As such, it needs to capture the effect of large concentrations of CO_2 and H_2O accurately. Hence, a CO sub-mechanism is also needed to capture CO_2's third-body effects and its potential decomposition to CO. Olm et al. compared 19 hydrogen and 16 syngas mechanisms [37,38] and ranked Keromnes et al.'s [32] as the best hydrogen and second best performing syngas oxidation mechanism in predicting a multitude of experimental validation targets. Keromnes et al.'s model is validated for 1-70 bar, 914-2220 K and equivalence ratios from 0.1 to 4.0. As such, this H_2/CO mechanism was selected as the "incumbent" starting model in this work. Its kinetic parameters for all reactions were reviewed and modified as needed, with particular focus on pressure-dependent reactions and third-body collider efficiencies pertinent to H_2O and CO_2. Following Alekseev et al. [39], FFCM-1 [40] and Hong et al. [41], an additional reaction, $H+HO_2=H_2O+O$, was added. Rate uncertainties and collision part-

ner efficiencies, when missing, were mostly extracted from FFCM-1 [40].

Table 1 illustrates the final evolved H_2/CO sub-mechanism, CanMECH 1.0, with "multiple-expression" treatment of pressure-dependent reaction rates using Troe formulation, when available. Relative to Keromnes et al. [32], the rates of reactions R2, R4-R6, R8-R10, R12-R15, R17, R20, R21, R23, R25-R30 were modified. However, Keromnes et al.'s [32] OH^* chemiluminescence reaction mechanism was adopted without any modification. The following paragraphs expound the reactions for which the rate parameters were modified relative to Keromnes et al. [32].

4.1. R2: $O+H_2=H+OH$

Keromnes et al. [32] used Sutherland et al.'s [43] rate over 504-2495 K. Baulch et al. [15] have noted that although Sutherland et al. [43] expression extrapolates well to the recent high temperature data, in the range of 1713-3532 K, their updated recommended rates improve the fit at the lower temperatures. As such, the dual rate expression, valid over 298-3300 K, recommended by Baulch et al. [15], is adopted in this work.

4.2. R4: $OH+OH=O+H_2O$

Keromnes et al. [32] adopted Sutherland et al.'s [43] rate for the reverse reaction. Hong et al. [69] evaluated this rate determination at above 1176 K and confirmed Woolridge et al.'s [47] results. Hashemi et al. [75] adopted Sangwan and Krasnoperov rate [87], who performed measurements at 295-414 K and 3 and 10 bar, and combined their results with Sangwan et al. [88] at 298-834 K and 1-100 bar, Bedjanian et al. [89] at 230-260 K, and Wooldridge et al. [47] at 1050-2380 K, to obtain a rate constant for 223-2380 K. Altinay and Macdonald [46] noted while their rate did not agree with Sangwan and Krasnoperov [87], it was in agreement with Nguyen and Stanton [90], Woolridge et al. [47] and Sutherland et al. [43] results. Altinay and Macdonald [46] fitted their 295-701 K results and Nguyen's theoretical data [90] and recommended a rate for 200-2000 K.

RMG identified this reaction to be pressure-dependent. Nguyen and Stanton [90] noted a potential for fall-off but recommended a low-pressure-limit rate. Sangwan et al. [88] provided the only pressure-dependent alternative in the literature but their He-based rate covered low temperatures of 298-834 K, and did not include collision efficiencies for H_2O or CO_2. Considering these features and Sangwan and Krasnoperov's [87] potentially underestimated rate [75], their rate was not adopted. Instead, Altinay and Macdonald's recommended rate [46] is used in this work.

4.3. R8: $H+OH(+M)=H_2O(+M)$

Li et al. [53] noted that because of the large uncertainty in this rate, laminar flame speed predictions using any particular set of diffusion coefficients can be forced to predict the same flame speed by adjusting the value of R8. RMG simulations identify this reaction as pressure-dependent. Keromnes et al. [32] reduced Li et al.'s recommended rate [53] by 8%. Li et al.'s rate was based on Tsang and Hampson's low-pressure-limit rate [49], increased by a factor of 1.72. As such, instead of this tuned rate, Sellevag et al.'s [91] Ar-based pressure-dependent rate, valid for 300-3000 K, along with their N_2-specific low-pressure-limit rate and collision efficiencies for other gases, was adopted in this work. Their theoretically derived rate fits various high-temperature rate data well, including Srinivasan and Michael [54]. FFCM-1 recommended collision efficiencies are utilized here [40]. For O_2, Burke et al. [25] collision efficiency was implemented. Due to the absence of collider efficiency for H_2O, a common efficiency of 14 relative to Ar was adopted in this work. FFCM-1 [40] also noted that Baulch et al.'s recommended rate [15] is slower than Srinivasan and Michael [54], bringing it closer to Sellevag et al. [91] which is reaffirming.

4.4. R9: $H+O_2(+M)=HO_2(+M)$

Troe [55], Bates et al. [56], Sellevag et al. [91], and Fernandes et al. [57] investigated the rate of this reaction but reported significantly different high-pressure-limit rate constants, k_∞, as well as center broadening factors F_{cent}. Bates et al. [56] investigated this rate behind reflected shock waves at 1050-1250 K and 7-152 bar. Bates et al. [56] also conducted a theoretical analysis, and reported reaction rates, centering factors, collider efficiencies, low- and high-pressure-limit rates for Ar, N_2 and H_2O. They noted H_2O to be 20 times more efficient as a collider than Ar, and that a very good fit was obtained to H_2O and N_2 but not for high-pressure Ar data.

Fernandes et al. [57] conducted rate determination experiments for M=He and N_2, and further analyzed the data of Hahn et al. [92] for Ar-based experiments at 300-700 K and 1-900 bar, as well as Janik et al. [93] experiments in H_2O at 350°C, to determine the fall-off parameters at 1.5-950 bar and 300-900 K. Fernandes et al. [57] also conducted theoretical calculations to extend the pressure and temperature range of validity. Klippenstein et al. [94] revisited this rate and supported the rates adopted by Burke et al. [25], as well as Fernandes et al.'s [57] theoretical rate determinations i.e., identical to Troe [55] for k_∞ and center broadening factors, F_{cent}. Consequently, Troe [55] rate is utilized for the high-pressure-limit rate in this study.

For the low-pressure-limit rate, Burke et al. [25] concluded that none of the recently proposed expressions [15,56,57,91,92] reproduced the observed pressure-dependence of the rate constant in Ar. Shao et al. [16] recently revisited the low-pressure-limit rates of R9 for colliders Ar, N_2, H_2O and CO_2. They conducted shock tube experiments of H_2-O_2 mixtures diluted in Ar, N_2, 14%H_2O/Ar and 20%CO_2/Ar. They combined these data with Bates et al. [56] and provided a revised low-pressure-limit rate with Troe's [55] temperature dependency. This H_2O-, CO_2-, Ar-, and N_2-specific rate expression is adopted in this work along with Burke et al. [25] FFCM-1 [40] collision efficiencies.

Because H_2O is a strong collider, Troe [55] recommends adopting a different formulation for its center broadening factor, F_{cent}. As F_{cent} of H_2O is temperature dependent and varied approximately between 0.73 and 0.87 [55], their average of 0.8 is adopted here.

4.5. R10: $H_2+O_2=H+HO_2$

We adopted the rate by Michael et al. [60], determined from ab initio calculations and validated by shock tube measurements of H_2-O_2 at 1600-2000 K. Keromnes et al. [32] reduced this rate by 30% to reduce the reactivity at low-temperatures while keeping the same reactivity at high temperatures. However, Keromnes et al.'s tuning is ignored here, because the rate of R10 is interrelated with R20, which was not included in Keromnes et al. [32], and is also interrelated with R14, for which a different rate was used as discussed in section 4.8. In-line with Hong et al. [41] and FFCM-1 [40], the untuned rate of Michael et al. [60] is used here.

4.6. R12: $HO_2+O=O_2+OH$

RMG identifies this reaction to be pressure-dependent. Keromnes et al. [32] utilized the rate by Baulch et al. [62]. Burke et al. [25] recently reviewed this rate and adjusted the A-factor of the theoretical ab initio-based rate of Fernandez et al. [63] by a factor of 0.6 to better fit the available measurements at

Table 1
CanMECH 1.0 syngas mechanism.

ID	Reaction	A	n	E_A (cal/mol)	UF	T range (K)	Ref.	Keromnes et al. [32]	Burke et al. [25]	Hong et al. [41]	FFCM-1 [40]	Alekseev et al. [39]+Konnov [27]	UF ref.
1	$H + O_2 = O + OH$	1.04E+14	0	1.531E+04	1.1	1100-3370	[42]	=	=	=	=	=	[42]
2	$O + H_2 = H + OH$	3.82E+12	0	7.949E+03	1.6	298-3300	[15]	[43]	=	=	=	[43]	[15]
		8.79E+14	0	1.918E+04	1.6	298-3300	[15]	NA	=	=	=	NA	[15]
3	$OH + H_2 = H + H_2O$	4.38E+13	0	6.991E+03	1.2	902-1518	[44]	=	[45]	[15]	[45]	[15]	[44]
4	$OH + OH = H_2O + O$	2.67E+06	1.82	-1.65E+03	1.4	200-2000	[46]	[43] rev	[15]	[47]	[15]	[27]	[46]
5	$H_2 + M = H + H + M$	4.58E+19	-1.4	1.0439E+05	3	600-2000	[48]	=	=	=	=	=rev*	[48]
	Relative to N_2: $\varepsilon_{He} = 0.83$, $\varepsilon_{CO2} = 3.8$, $\varepsilon_{CO} = 1.9$, $\varepsilon_{Ar} = 0$, $\varepsilon_{H2} = 0$, $\varepsilon_{H2O} = 0$						[32]						
	$H_2 + H_2 = H + H + H_2$	8.61E+17	-0.7	1.0439E+05	3	600-5000	[48]	NA	=	=	=	=rev	[48]
	$H_2 + H_2O = H + H + H_2O$	8.61E+19	-1.1	1.0439E+05	5	600-2000	[48]	NA	=	=	=	=rev	[48]
	$H_2 + Ar = H + H + Ar$	5.84E+18	-1.1	1.0439E+05	2	600-5000	[48]	NA	=	=	=	=rev	[48]
6	$O + O + M = O_2 + M$	6.2E+15	-0.5	0E+00	3	2000-10000	[49]	=	=	=	=	[50]	
	Relative to N_2: $\varepsilon_{He} = 0.83$, $\varepsilon_{H2} = 2.5$, $\varepsilon_{H2O} = 12$, $\varepsilon_{CO2} = 3.8$, $\varepsilon_{CO} = 1.9$, $\varepsilon_{Ar} = 0$, $\varepsilon_{O2} = 0$												
	$O + O + Ar = O_2 + Ar$	1.9E+13	0	-1.79E+03	3	200-4000	[49]	NA	=	=	=	NA	[15]
	$O + O + O_2 = O_2 + O_2$	8.0E+19	-1.5	0E+00	3	2000-10000	[49]	NA	NA	NA	NA	NA	[15]
7	$O + H + M = OH + M$	4.7E+18	-1	0E+00	5	300-3000	[49]	=	=	=	=	[51]	[15]
	Relative to N_2: $\varepsilon_{He} = 0.75$, $\varepsilon_{CO2} = 3.8$, $\varepsilon_{CO} = 1.9$, $\varepsilon_{Ar} = 0.75$, $\varepsilon_{H2} = 2.5$, $\varepsilon_{H2O} = 12$												
8	$H + OH (+M) = H_2O (+M)$	2.51E+13	0.234	-1.14E+02	2	300-3000	[91]	[53]	[54] rev	[54] rev	[54] rev	[54] rev	[91]
	Ar Low Pressure Limit	3.1E+20	-1.527	3.68E+02	2	300-3000	[91]	NA	NA	NA	NA	NA	[91]
	For Ar: $F_{cent} = 0.72$, $T^{***} = 1.00E\text{-}30$, $T^{*} = 1.00E+30$, $T^{**} = 1.00E+30$												
	Relative to Ar: $\varepsilon_{He} = 1.1$, $\varepsilon_{H2} = 3$, $\varepsilon_{O2} = 1.5$, $\varepsilon_{N2} = 0$, $\varepsilon_{H2O} = 14$, $\varepsilon_{CO2} = 3.8$, $\varepsilon_{CO} = 1.9$,						[91]						
	N_2 low pressure limit	4.53E+21	-1.81	4.99E+02		300-3000	[91]	NA	NA	NA	NA	NA	[91]
	For N_2: $F_{cent} = 0.73$, $T^{***} = 1.00E\text{-}30$, $T^{*} = 1.00E+30$, $T^{**} = 1.00E+30$						[91]						
9	$H + O_2 (+M) = HO_2 (+M)$	4.7E+12	0.44	0E+00	1.2	300-2000	[55]	=	=	[56]	=	=	[55]
	N_2 low pressure limit	1.2E+19	-1.2	0E+00	1.12	1000-1400	[16]	[57]	[58]	[56]	[25]	=	[16]
	For N_2: $F_{cent} = 0.5$, $T^{***} = 1.00E\text{-}30$, $T^{*} = 1.00E+30$, $T^{**} = 1.00E+30$							[57]	[58]	[56]	[59]	=	
	Relative to N_2: $\varepsilon_{He} = 0.8$, $\varepsilon_{H2} = 2$, $\varepsilon_{O2} = 0.78$, $\varepsilon_{N2} = 0$, $\varepsilon_{H2O} = 0$, $\varepsilon_{CO2} = 0$, $\varepsilon_{CO} = 1.9$, $\varepsilon_{Ar} = 0$						[55]	[57]	[25]	[58]			
	Ar Low Pressure Limit	7.8E+18	-1.2	0E+00	1.12	1000-1400	[16]x0.88	[56]	[58]	[56]	NA	NA	[16]
	For Ar: $F_{cent} = 0.5$, $T^{***} = 1.00E\text{-}30$, $T^{*} = 1.00E+30$, $T^{**} = 1.00E+30$						[55]	[56]	[25]	[56]			
	H_2O low Pressure limit	2.04E+20	-1.2	0E+00	1.24	1000-1400	[16]	NA	NA	[56]	NA	NA	[16]
	For H_2O: $F_{cent} = 0.8$, $T^{***} = 1.00E\text{-}30$, $T^{*} = 1.00E+30$, $T^{**} = 1.00E+30$						[55]			[56]			
	CO_2 low pressure limit	4.43E+19	-1.2	0E+00	1.19	1000-1400	[16]	NA	NA	NA	NA	NA	[16]
	For CO_2: $F_{cent} = 0.5$, $T^{***} = 1.00E\text{-}30$, $T^{*} = 1.00E+30$, $T^{**} = 1.00E+30$						[55]						
10	$H_2 + O_2 = H + HO_2$	7.395E+05	2.4328	5.3507E+04	2	400-2300	[60]	= x 0.7	=rev x 0.75	=rev	=rev	=	[40]
11	$HO_2 + H = OH + OH$	7.08E+13	0	2.95E+02	2	300-2000	[61]	=	=	=	=	=	[40]
12	$HO_2 + O = OH + O_2$	2.85E+10	1	-7.239E+02	2	300-2500	[25]	[62]	= [63] x 0.6	[15]	[15]	=	[39]
13	$HO_2 + OH = H_2O + O_2$	7.0E+12	0	-1.09E+03	1.67	250-2200	[64]	[65] x 0.85	[65]	[62]	=	=	[64]
		4.5E+14	0	1.093E+04	1.67	250-2200	[64]					=	[64]
14	$HO_2 + HO_2 = H_2O_2 + O_2$	1.03E+14	0	1.104E+04	1.67	300-1283	[66]	[67] x 0.87	[67]	[67]	=	=	[64]
		1.94E+11	0	-1.41E+03	1.67	300-1283	[66]	[67]	[67]	[67]	=	=	[64]

(*continued on next page*)

Table 1 (*continued*)

ID	Reaction	A	n	E_A (cal/mol)	UF	T range (K)	Ref.	Keromnes et al. [32]	Burke et al. [25]	Hong et al. [41]	FFCM-1 [40]	Alekseev et al. [39]+Konnov [27]	UF ref.
15	H_2O_2 (+M) = OH + OH (+M)	2.0E+12	0.9	4.8754E+04	2	500-1500	[68]	=	=	[52]	=	=	[68]
	AR low pressure limit	2.5E+24	-2.3	4.8754E+04	2	500-1500	[68]	=	=	[69,70]	=	=	[68]
	For Ar: F_{cent} = 0.42, T^{***} = 1.00E-30, T^{*} = 1.00E+30						[68]	=F_{cent} = 0.43	=		=	=	[68]
	Relative to Ar: ε_{He} = 1.1, ε_{H2} = 3.7, ε_{O2} = 1.2, ε_{N2} = 0, ε_{H2O} = 0, ε_{CO2} = 0, ε_{CO} = 1.9, ε_{H2O2} = 0						[68]	=	=	[70,71,72]	=	=ε_{H2O2}=7.7	[68]
	H_2O low Pressure limit	1.9E+25	-2.3	4.8754E+04	2	500-1500	[68]	=	NA	NA	NA	NA	[68]
	For H_2O: F_{cent} = 0.51, T^{***} = 1.00E-30, T^{*} = 1.00E+30						[68]	=					[68]
	H_2O_2 low pressure limit	1.9E+25	-2.3	4.8754E+04	2	500-1500	[68]	NA	NA	NA	NA	NA	[68]
	For H_2O_2: F_{cent} = 0.51, T^{***} = 1.00E-30, T^{*} = 1.00E+30						[68]						[68]
	CO_2 low pressure limit	3.9E+24	-2.3	4.8754E+04	2	500-1500	[68]	NA	NA	NA	NA	NA	[68]
	For CO_2: F_{cent} = 0.43, T^{***} = 1.00E-30, T^{*} = 1.00E+30						[68]						[68]
	N_2 low pressure limit	3.7E+24	-2.3	4.8754E+04	2	500-1500	[68]	NA	NA	NA	NA	NA	[68]
	For N_2: F_{cent} = 0.43, T^{***} = 1.00E-30, T^{*} = 1.00E+30						[68]						[68]
16	$H_2O_2 + H = H_2O + OH$	2E+13	0	3.974E+03	5	300-1000	[49]	=	=	[15]	=	[73]	[49]
17	$H_2O_2 + H = H_2 + HO_2$	5E+13	0	7.949E+03	5	300-1000	[49]	[73] mod	=	[59]	=	[73]	[49]
18	$H_2O_2 + O = OH + HO_2$	9.6E+06	2	3.974E+03	3	500 & above	[49]	=	=	3	=	=	[49]
19	$H_2O_2 + OH = H_2O + HO_2$	1.738E+12	0	3.18E+02	2	280-1640	[69]	=	=	=	=	=	[40]
		7.586E+13	0	7.273E+03	1.3	280-1640	[69]	=	=	=	=	=	[40]
20	$HO_2 + H = H_2O + O$	1.4E+12	0	0E+00	3	298	[15]	NA	NA	=	=	58	[40]
CO Sub-mechanism								Keromnes et al. [32]	Li et al. [74]	Hashemi et al. [75]	FFCM-1 [40]		
21	CO+ O (+M) = CO_2(+M)	1.8E+10	0	2.43E+03	10	298-3500	[76]	= x 0.75 + E_A x 0.98	= E_A x 0.98	=	=		[40]
	N_2 low pressure limit	1.4E+21	-2.1	5.5E+03	10	298-3500	[76]	[77] x 0.87	[77]	=	=		[40]
	For N_2: F_{cent} = 1						[40]	=	=	=	=		
	Relative to N_2: ε_{H2} = 2.5, ε_{Ar} = 0.87, ε_{CO2} = 3.8, ε_{CO} = 1.9, ε_{H2O} = 12							=ε_{He} = 0.7, ε_{Ar} = 0.7	=	ε_{Ar} = 1	=		
22	CO + O_2 = CO_2 + O	2.5E+12	0	4.7693E+04	10	1500-3000	[49]	=	=	[75]	=		[40]
23	CO + OH = CO_2 + H	7.05E+04	2.053	-2.76E+02	1.2	300-2500	[78]	= x 1.29	[74]	[79]	= x 1.29		[40]
		5.76E+12	-0.664	3.32E+02	1.5	300-2500	[78]	NA	NA	NA	=		[40]
24	CO + HO_2 = CO_2 + OH	1.57E+05	2.18	1.794E+04	2	300-2500	[80]	=	[61]	=	=		[80]
25	HCO(+M)=H+CO(+M)	4.93E+16	-0.93	1.973E+04		300-2700	[81]	NA	NA	=	NA		
	Ar low pressure limit	7.43E+21	-2.36	1.939E+04		300-2700	[81]	NA	NA	=	[82]		
	For Ar: α = 0.103, T^{***} = 139, T^{*}=1.09E4, T^{**}=4.55E3						[81]			=			
	Relative to Ar: ε_{He} = 1.3, ε_{H2} = 2, ε_{O2} = 1.5, ε_{N2} = 1.5, ε_{H2O} = 15, ε_{CO2} = 3, ε_{CO} = 1.5						[83]	ε's mod	ε's mod	=	ε's mod		
26	HCO + O_2 = CO + HO_2	6.92E+06	1.90	-1.37E+03		295-1705	[84]	[85]	[85]	=	[40]		
27	HCO + H = CO + H_2	9.0E+13	0	0E+00	2.5	298-2500	[15]	[86]	[86]	[82]	=		[15]
28	HCO + O = CO + OH	3E+13	0	0E+00	2	300-2500	[15]	[49]	[49]	[62]	=		[15]
29	HCO + O = CO_2 + H	3E+13	0	0E+00	2	300-2500	[15]	[49]	[49]	[62]	=		[15]
30	HCO + OH = CO + H_2O	1.1E+14	0	0E+00	2	296-2500	[15]	[62]	[49]	=	=		[15]
31	HCO + HO_2 = CO_2 + H + OH	3.0E+13	0	0E+00	5		[49]	=	=	=	NA		[49]
32	HCO + HCO = H_2 + CO + CO	3.0E+12	0	0E+00	1.5		[49]	=	=	NA	NA		[49]

Note: Rate constant has units of cm^3/mol/s/cal.
LEGEND: "ref": Reference, "UF": Uncertainty Factor, "=": Same rate parameters; "rev": Reverse rates; "NA": Not Available.

low temperatures. Burke et al. [25] recommended rate is adopted in this work.

4.7. R13: $HO_2+OH=H_2O+O_2$

Keromnes et al. [32] reduced Keyser's [65] rate by 15% and noted that due to an unusual non-Arrhenius behaviour of this reaction as it goes through a minimum around 1250 K, some have used up to five expressions to reproduce the temperature dependence. However, two recent experimental and theoretical studies of Hong et al. [64] and Burke et al. [95] re-evaluated this rate expression, and significantly reduced the associated uncertainty. Hong et al. [64] did not find strong temperature dependency, and recommended a two-expression rate by fitting their experimental data. The authors mentioned this is in good agreement with Burke et al. theoretical study [95]. Hong et al.'s [64] rate is adopted in this work.

4.8. R14: $HO_2+HO_2=H_2O_2+O_2$

The double-expression Arrhenius rate from Hong et al. [64] which confirms Kappel et al.'s [66] rate is selected in this work. Kappel et al. conducted shock tube experiments at 950-1250 K and included low temperature data to recommend rate expression for 300-1250 K. Hong et al. [64] recently conducted shock tube studies in the range of 1072-1283 K. Since their results were in good agreement with Troe's shock tube experiments at 950-1450 K [96] as well as Kappel et al.'s rate, the latter rate is retained for this reaction. The temperature validation range is increased to 300-1283 K by Hong et al. [64].

4.9. R15: $H_2O_2\ (+M) = OH + OH\ (+M)$

Keromnes et al. [32] utilized the rate by Troe [68] but modified Ar broadening factor and did not include collider-specific rates for H_2O_2, CO_2, and N_2. Here, the same pressure-dependent Ar-based rate is used along with Troe's [68] low-pressure-limit-rates and broadening factors for H_2O, CO_2, H_2O_2, and N_2. The multiple-expression treatment of this pressure-dependent rate is important to this work's high-pressure conditions involving high concentrations of H_2O, considering ~20% higher broadening factor of H_2O relative to Ar used in single-expression alternatives. Sajid et al. [97] measured the rate of R15 at pressures of 1, 2 and 10 atm at 930-1235 K in Ar, and recommended a rate within the error bounds of the rate from Troe [68].

4.10. R17: $H_2O_2 + H = H_2 + HO_2$

This H-abstraction channel of H_2O_2's reaction with H radical is interconnected with R16: $H_2O_2+H=H_2O+OH$. Keromnes et al. [32] used the theoretical rate by Ellingson et al. [73]. Lu et al. [98] recently revisited R17 rate and proposed a new theoretically determined rate. Superimposing Lu et al.'s [98] rate with Keromnes et al. [32], Alekseev et al. [39], and Tsang and Hampson [49], reveals these rates are very different, see Fig. S9. Based on IDT sensitivity analyses, it is observed that rates smaller than those of Tsang and Hampson [49] are needed at temperatures of 1225 K to obtain a reasonable fit of the new high-pressure H_2O-laden validation data in this work. As such, Tsang and Hampson rate is adopted in this work.

4.11. R20: $HO_2+H=H_2O+O$

Burke et al. [25] estimated this reaction to be potentially responsible for less than 14% of the flux of $H+HO_2$, but they noted that inclusion of this reaction yields substantially faster oxidation rates at flow reactor and high-pressure flame conditions. The authors noted a few shortcomings of their theoretical calculations rendering them inconclusive and opted to exclude it, deeming R10 and R11 branches of $H+HO_2$ to be responsible for the majority of the flux. Konnov et al. [99] showed that R11 and this reaction, although not important in slow H_2 oxidation processes, have opposite signs in laminar flame sensitivities and retained this reaction. In this study, in-line with Konnov et al. [99], Hong et al. [41], and FFCM-1 [40], Baulch et al.'s [15] recommended rate is adopted.

4.12. R21: $CO+O(+M)=CO_2(+M)$

Keromnes et al. [32] and Li et al. [74] both implemented Troe's [76] rate, but modified its activation energy. Keromnes et al. [32] reduced the rate by a factor of 0.75 but a recent theoretical study by Jasper and Richard [100] suggests an even higher rate than Troe [76]. As such, in this study, the untuned rate of Troe [76] is utilized. As collider-specific rate constants are not available, a single expression Troe formulation is the only choice, and FFCM-1 [40] relative efficiencies sourced from Li et al. [74] are adopted. For the fall-off behaviour, in-line with FFCM-1 [40], Lindemann fall-off with $F_{cent}=1$ is assumed. For the low-pressure-limit rate, both Keromnes et al. [32] and Li et al. [74] refer to the theoretical rate of Westmoreland et al. [77]; while Keromnes et al. [32] reduced the rate, Li et al. [74] retained the original pre-exponential factor. In this work Troe [76] untuned low-pressure-limit rate is used.

4.13. R25: $HCO\ (+M) = H + CO\ (+M)$

For this pressure-dependent reaction rate, Keromnes et al. [32] utilized a low-pressure-limit rate from Li et al. [74]. FFCM-1 [40] adopted Friedrichs et al. [82] theoretical RRKM calculated rates, fitted to shock tube data with Ar bath gas at 1000 K for the decomposition of formaldehyde, with relative efficiencies from GRIMech [59]. However, this rate is also at the low-pressure-limit. As the focus of this study is to ensure pressure dependence is properly captured in the presence of strong colliders such as CO_2 and H_2O, the theoretical rate of Yang et al. [81], in-line with Hashemi et al. mechanisms [75,83], is adopted in this study. Yang et al. [81] conducted a theoretical study and calculated a pressure dependent rate covering a pressure range of 0.01-1000 atm at 300-2700 K. The enhanced third-body collider efficiencies were adopted from Hashemi et al. mechanism [75].

4.14. R26: $HCO+O_2=CO+HO_2$

Keromnes et al. [32], Li et al. [74], and Metcalfe et al. [101] adopted Timonen et al.'s 1988 rate [85]. Alternatively, FFCM-1 [40] used a rate referring to communications with Klippenstein, which was slower. Hashemi et al. [75] utilized the more recent rate of Faßheber et al. [84], involving HCO concentration measurements behind Ar diluted shockwaves of glyoxal pyrolysis at temperatures of 1285-1760 K. Faßheber et al. [84] combined their data with low-temperature data from the literature to produce a more inclusive rate applicable to the temperature range of 295-1705 K. In-line with Hashemi et al. [75], this more recent rate involving higher temperature experimental data at combustion relevant temperatures is adopted instead of Timonen et al. [85].

4.15. Other modifications

For R5: $H_2+M=H+H+M$, in addition to the N_2-based rate expression from Cohen and Westberg's review [48], their collider specific rates for H_2, Ar and H_2O are added as they have different temperature dependencies than N_2. Similarly, for R6:

O_2+M=O+O+M, additional collider-specific rates from Tsang and Hampson [49] are added for O_2 and Ar due to their differing temperature dependencies as compared to the N_2-based rate expression of the same source.

For the four radical recombination reactions involving HCO and H, O, and OH, i.e., R27: HCO+H=CO+H_2, R28: HCO+O=CO+OH, R29: HCO+O=CO_2+H, and R30: HCO+OH=CO+H_2O, more recent rate recommendations by Baulch et al. [15] are adopted.

5. Experimental facilities

The high-pressure shock tube (HPST) and low-pressure shock tube (LPST) test facilities at King Abdullah University of Science and Technology (KAUST) were used for IDT measurements in this work. HPST facility, previously described by Alabbad et al. [102], has a constant internal diameter of 10 cm, a 6.6 m long driven section, and a 2.2 m long driver section. The shock tube, its feed line and mixing vessel (MV) were heated to 150°C for H_2O- and CO_2-laden tests. Six piezoelectric PCB 112A05 pressure transducers coupled with Agilent 53220A 100ps frequency counters measured the incident shock velocity over the last 3.7 meters of the driven section. To measure side-wall P_5, a Kistler 603B1 piezoelectric pressure transducer located at 10.48 mm from the end-wall was used. The data acquisition (DAQ) system included a 15-bit National Instruments BNC-2110 and a Tektronix DPO 3014 Digital Phosphor Oscilloscope.

The LPST facility, previously described by Badra et al. [103] has a 9-meter-long driver and driven sections, with an inner diameter of 14 cm. Five piezoelectric PCB pressure transducers, located over the last 1.5 m of its driven section, coupled with Agilent 53220A, measured the incident shock velocity. A Kistler 603B piezoelectric pressure transducer measured the post-reflected shock pressure P_5, located at 2 cm from the end-wall. The DAQ system included a National Instruments BNC-2110 15-bit and a Tektronix DPO 4104B Digital Phosphor Oscilloscope.

For accurate determination of time zero in bifurcating mixtures of this work, a fixed wavelength continuous-wave IR laser at 3392 nm or a continuous wave UV laser at 306 nm was used.

For ignition time determinations, side-wall and end-wall OH* emissions were detected using HAMAMATSU 1P21 photomultipliers with THORLABS 307 bandpass filters. Side-wall OH* emission was the main diagnostic used for IDT determinations. For HPST and LPST, dp/dt was estimated to be in the range of 2-3.5%/ms for the experiments reported herein.

To minimize impurities effects, the mixture preparation apparatus was cleaned with tert-Butyl hydroperoxide (TBHP) or acetone, and vacuum pumped overnight to lower than 10^{-4} milli-bar. LPST and HPST cleaning with acetone and TBHP was followed with five unfueled high concentration oxygen shocks at temperatures of 3000-5000 K to burn off any remaining cleaning agent, and vacuum pumped to lower than 10^{-4} milli-bar.

Certified high-purity gases, namely: H_2 (≥ 99.9999%), O_2 (≥ 99.999%), Ar (≥ 99.9999%), He (99.999%), CO_2 (≥99.995%) were sourced from Abdullah Hashim Gases (AHG). Mixtures were prepared manometrically. For H_2O-laden mixtures in the HPST, MV was heated to 150°C. Water was injected using a Monoject hypodermic syringe (0.813 mm x 3.8 cm) and septa valve, following H_2 and O_2 injection. Complete vaporization of H_2O was monitored until the mixing vessel pressure rise plateaued, and was followed by CO_2 and Ar injection, respectively.

To determine T_5 and P_5, the FROSH code [104] was adopted. Inputs to the code are the measured values of pre-test driven section temperature and pressure T_1, P_1, the measured incident shock velocity, and thermodynamic properties and composition of feed gases. In these calculations, the effect of deviations from ideal gas behaviour on thermodynamic properties, and mixture concentrations containing H_2O and CO_2 were non-negligible and were accounted for in the reported uncertainties. An in-house code was developed to automate the calculation of uncertainties, similar to Campbell [104].

6. Experimental results

Experimental IDT is defined as the time delay between the laser Schlieren spike, signifying the arrival of the reflected shockwave, i.e., time zero (t_0), and the ignition time (t_{ign}) determined as the intersection of the tangent to either of side-wall or end-wall OH* emissions' highest-slope inflection with their baseline values after the passage of the reflected shock (see Fig. S48). This definition of ignition time (t_{ign}) was also applied to side-wall pressure trace.

Table S2 and Table S3 detail the results of low- and high-pressure experimental IDT measurements of 4%H_2/2%O_2 in Ar, in 45%CO_2/Ar, in 45%H_2O/Ar, and in 30%H_2O/15%CO_2/Ar. Figures S10-S60 depict the associated test-specific raw data utilized for IDT determinations for the 51 experiments of this work. End-wall OH* emission was the signal of choice for low-pressure IDT reporting, whereas side-wall OH* emission was used for the reported high-pressure IDT determinations. While end-wall emission is deemed to be a preferred diagnostic for mixtures with high concentrations of triatomic bath gas, our side-wall emission provided a clearer / sharper indication of the onset of ignition in high-pressure experiments. IDT estimates from the different diagnostics corroborate reasonably well (see Fig. S61 to Fig. S63). IDTs using side-wall pressure were only reported for Ar-diluted experiments due to low signal-to-noise ratio and bifurcation effects, signified by two peaks and valleys, observed for H_2O- and CO_2-laden mixtures.

Uncertainties in reported IDTs stem from ignition delay determinations (time zero and ignition time) as well as uncertainties in T_5 and P_5 calculations. Time zero (t_0) determination using laser Schlieren had negligible uncertainty for most experiments. t_{ign} uncertainties were test-specific and of the order of 1% for Ar, 2% for 45%CO_2/Ar-diluted experiments, and ~5% for H_2O-laden tests. The first rise of side-wall OH* emission was often not the steepest for high-pressure 45%H_2O-laden tests, which had multiple inflections. While the reported IDTs were based on steepest-rise inflection point, unbalanced vertical error bars were extended to include IDT estimates determined from tangent to the inflection of first rise in OH* emission. Combined t_0 and t_{ign} determination uncertainties are summarized in Table S4 and Table S5 for the low- and high-pressure ignition delay campaigns.

T_5 and P_5 calculated uncertainties included T_1, P_1, incident shock velocity, gas properties and their deviations due to pressure dependency, H_2O and CO_2 concentrations and additional uncertainties due to non-ideal gas mixtures P-V-T behaviour. The uncertainties were determined using root-sum-of-squared (RSS) method [104] (see Table S4 and Table S5). RSS uncertainty calculation requires errors to be random and orthogonal. The latter is satisfied due to the small errors in temperature although other inputs depend on temperature. For the former, at high pressures, C_p values of H_2O and CO_2 and concentration uncertainties are highly skewed and were in the same direction due to the deviation from ideal gas behaviour. As C_p and concentration errors were of the same order and in the same direction, RSS errors bars were deemed appropriate since the positive and negative RSS uncertainties are calculated independently which enables them to capture the skew in error. RSS errors were also used in graphical representations of IDTs.

7. Model validation and parameter tuning results

To evaluate the effectiveness of kinetic models in reproducing IDT validation targets, two performance evaluation metrics based on relative errors are used. This precludes any bias toward larger

IDTs with larger absolute errors. As a measure of the average relative prediction error, Root Mean Square Relative Error (RMSRE) was utilized to evaluate model performance, according to:

$$RMSRE = \sqrt{\frac{\sum_{i=1}^{n}\left(\frac{IDT_{predicted,\ i} - IDT_{Measured,\ i}}{IDT_{Measured,i}}\right)^2}{n}} \quad (1)$$

where $i = 1..N$ is the index of each data point within a dataset of size N

Another metric, the relative percent RMSRE or RPRMSRE is a measure of improvement in performance, in percentage, for the developed model relative to the incumbent:

$$RPRMSRE = \frac{RMSRE_{model} - RMSRE_{incumbent}}{RMSRE_{incumbent}} \times 100\% \quad (2)$$

To develop a model with minimal parameter tuning, the performance of the incumbent Keromnes et al. and untuned CanMECH Base models were evaluated and compared. Datasets that CanMECH Base did not predict as well as Keromnes et al. were identified. To distinguish the appropriate reaction rate parameter(s) for tuning, IDT sensitivity analyses were carried out which evaluated the effect of adjusting pre-exponential factors, collision efficiencies and center broadening factors of pressure-dependent reactions. Both performance evaluation criteria were monitored, and predictions for individual subsets of data as well as the complete validation dataset were compared. The extent of tuning was limited to the uncertainty bounds provided by the source study of rate parameter(s). The resulting updated model, CanMECH 1.0, is the minimally tuned and improved mechanism for H_2/CO combustion modeling in this work.

In addition to the experimental IDT data of this work, shock tube IDT validation datasets from Shao et al. [16], Pang et al. [31], Ninnemann et al. [30] and Keromnes et al. [32] were used to evaluate the performance of the developed models.

Table 2 details the values of the performance evaluation metrics for the three models, namely: the untuned CanMECH Base, CanMECH 1.0, as well as the incumbent, Keromnes et al. [32].

Table 2 is divided into various datasets. Within each dataset, each row is dedicated to a subset of data conducted at similar conditions but spanning different temperature ranges. Each row details the conditions explored, and RMSRE and RPRMSRE values. Yellow cells identify the best performing model, i.e., with lowest RMSRE, for each subset. Orange cells identify the best performing model for a complete dataset. The cell, with the red fill on the last row indicates the model with the best overall performance. The green cells in the last column distinguish subsets where CanMECH 1.0 has an improved or identical performance relative to the incumbent [32]. Based on the definition of RPRMSRE, a more negative value translates to a larger percentage reduction of the overall RMSRE brought about by the adoption of CanMECH 1.0 in place of the incumbent mechanism.

Model performance is also examined graphically. Experimental results' vertical error bars represent t_0 and t_{ign} uncertainties, and horizontal bars indicate RSS uncertainties of $1000/T_5$. Figure 1 illustrates measured IDTs for 4%H_2/Ar at equivalence ratio (φ) of 1, 926-1198 K and 2.1-2.4 bar, as well as modelled IDTs at 2.25 bar. All models generally predict the data well; however, they overpredict measured IDTs at temperatures above 1000 K, with Keromnes et al. [32] reproducing the data better than other models. CanMECH Base shows the largest deviation from experimental data at temperatures above 1000K, with an RMSRE of 0.257 vs. 0.233 for Keromnes et al. [32].

Figure 2 depicts 4%H_2/45%CO_2/Ar φ=1 measured IDTs at 1061-1150 K and 2.4-2.7 bar, in addition to modelled IDTs at 2.5 bar. Keromnes et al. [32] overestimates the measured IDTs across the explored temperature range, whereas CanMECH base reproduces the experimental data more closely, in particular at temperatures below ~1100 K. In the presence of CO_2, CanMECH Base performs better than the incumbent, signified by its lower RMSRE, i.e., 0.287 vs. 0.685.

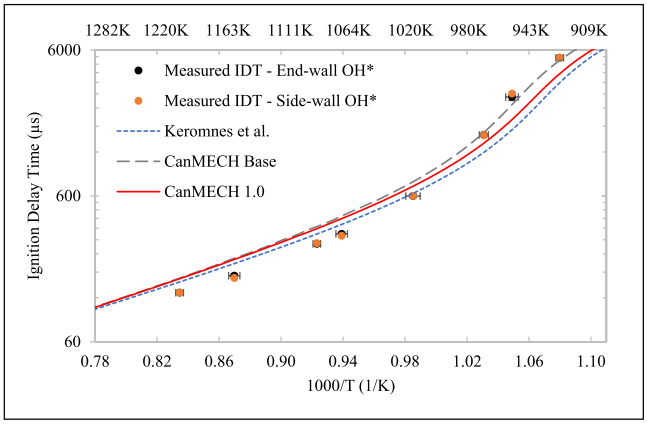

Fig. 1. Measured IDTs for 4%H_2/Ar, φ=1, at 2.1-2.4 bar, modelled IDTs at 2.25 bar.

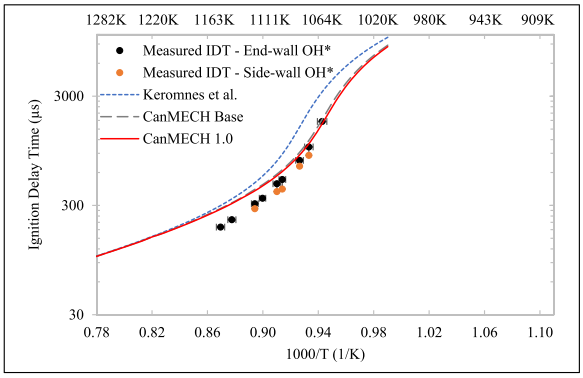

Fig. 2. Measured IDTs for 4%H_2/45%CO_2/Ar, φ=1 at 2.4-2.7 bar, modelled IDTs at 2.5 bar.

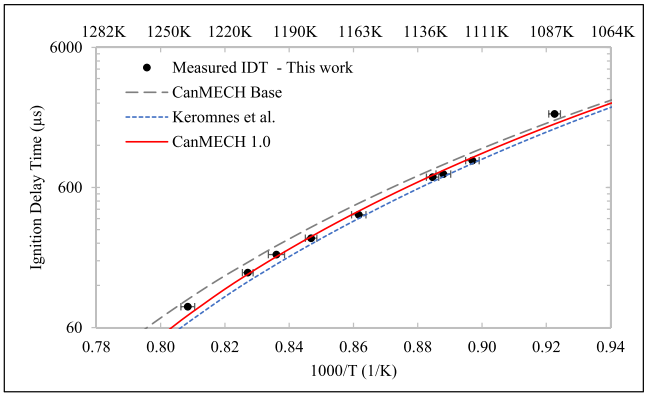

Fig. 3. Measured IDTs for 4%H_2/Ar, φ=1 at 37-43.8 bar, modelled IDTs at 40 bar.

Figure 3 plots measured IDT results for 4%H_2/Ar φ=1 at 1084-1237 K and 37-43.8 bar, as well as modelled IDTs at 40 bar. Figure 3 and RMSRE values (Table 2) show that the incumbent performs better than CanMECH Base. The incumbent mechanism underestimates the IDTs while CanMECH Base over-estimates them. Comparison of Figs. 1 and 3 reveals that model performance improved at higher pressure with ~50% lower RMSREs.

Figure 4 depicts 4%H_2/45%H_2O/Ar φ=1 measured IDTs at 1106-1242 K and 39.1-40.7 bar, as well as modelled IDTs at 40 bar.

Table 2
Model performance evaluation results matrix.

Dataset ID	Source	Fuel & Bath gas Composition	# of data	Pressure range (bar)	Temperature range (K)	φ	CanMECH 1.0 RMSRE	CanMECH Base RMSRE	Keromnes et al. RMSRE	CanMECH 1.0 vs. Keromnes et al. RPRMSRE (%)
1	This Work	4%H_2/Ar	8	2.1-2.4	926-1198	1	0.246	0.257	0.233	6
		4%H_2/45%CO_2/Ar	9	2.4-2.7	1061-1150	1	0.262	0.287	0.685	-62
		Combined at ~ 2.4bar	**17**	**2.1-2.7**	**926-1198**	**1**	**0.255**	**0.273**	**0.523**	**-51**
2	This Work	4%H_2/Ar	9	37.0-43.8	1084-1237	1	0.067	0.169	0.122	-45
		4%H_2/45%H_2O/Ar	8	39.1-40.7	1106-1242	1	0.192	0.192	0.269	-29
		4%H_2/30%H_2O/15%CO_2/Ar	8	40.4-41.6	1108-1232	1	0.097	0.097	0.179	-46
		4%H_2/45%CO_2/Ar	9	39.3-43.8	1133-1226	1	0.075	0.080	0.075	0
		Combined at ~ 40bar	**34**	**37.0-43.8**	**1084-1242**	**1**	**0.116**	**0.142**	**0.173**	**-33**
3	Shao et al. [16]	3%H_2/Ar	5	29.1-32.9	1230-1262	1	0.382	0.134	0.453	-16
		3%H_2/Ar	6	17.0-17.6	1184-1224	1	0.243	0.091	0.315	-23
		3%H_2/N_2	5	12.8-13.3	1199-1228	1	0.162	0.162	0.313	-48
		3%H_2/4.4%H_2O/Ar	3	15.9-17.0	1264-1307	1	0.185	0.247	0.348	-47
		3%H_2-9%H_2O-Ar	6	15.2-16.6	1270-1344	1	0.166	0.230	0.354	-53
		3%H_2/13.4%H_2O/Ar	2	15.3-15.7	1282-1376	1	0.093	0.133	0.377	-75
		3%H_2/20%CO_2/Ar	11	11.7-19.3	1185-1268	1	0.203	0.221	0.408	-50
		3%H_2/10%CO_2/Ar	2	11.4-11.9	1179-1180	1	0.294	0.146	0.150	96
		Combined	**40**	**11.4-32.9**	**1179-1376**	**1**	**0.231**	**0.186**	**0.367**	**-37**
4	Pang et al. 2009 [31]	**4%H_2/Ar**	**33**	**3.42-3.76**	**924-1118**	**1**	**0.332**	**0.651**	**0.238**	**40**
5	Ninnemann et al. [30]	**4%H_2/Ar**	**10**	**3.13-5.51**	**960-1131**	**1**	**0.332**	**0.458**	**0.253**	**27**
6	Keromnes et al. (S11) [32]	3.47%H_2/N_2	11	0.94-1.05	932-1954	0.5	0.282	0.282	0.245	15
			13	3.91-4.54	1006-1257	0.5	0.313	0.313	0.490	-36
			10	15.1-16.3	1060-1243	0.5	0.321	0.321	0.251	28
		Combined- S11	**34**	**0.94-16.3**	**932-1954**	**0.5**	**0.306**	**0.306**	**0.360**	**-15**
7	Keromnes et al. (S12) [32]	12.54%H_2/Ar	26	0.92-1.37	943-2136	4	0.208	0.210	0.207	0
			20	3.7-4.5	967-1463	4	0.129	0.232	0.182	-29
			16	14.2-16.6	947-1227	4	0.248	0.286	0.242	3
		Combined-S12	**62**	**0.92-16.6**	**943-2136**	**4**	**0.199**	**0.239**	**0.209**	**-5**
8	Keromnes et al. (S13) [32]	**2.98%H_2/0.52%CO/46.57%N_2/46.42%Ar**	7	15.0-16.6	1002-1222	**0.5**	**0.443**	**0.453**	**0.455**	**-3**
9	Keromnes et al. (S16) [32]	2.96%H_2/2.96%CO/Ar	23	0.76-1.18	924-2220	1	0.240	0.231	0.199	20
			23	3.71-5.07	942-1364	1	0.202	0.204	0.226	-11
			16	14.7-16.8	997-1215	1	0.245	0.329	0.225	9
		Combined-S16	**23**	**0.76-16.8**	**924-2220**	**1**	**0.228**	**0.251**	**0.216**	**5**
Overall			**299**	**0.76-43.8**	**924-2220**	**0.5-4**	**0.250**	**0.324**	**0.289**	**-14**

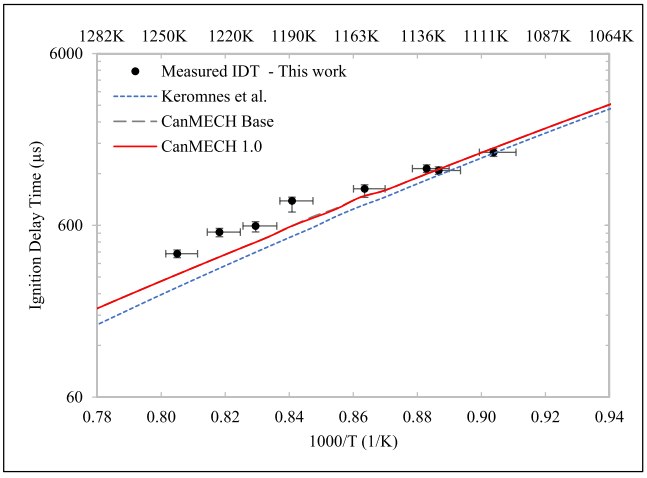

Fig. 4. Measured IDTs for 4%H_2/45%H_2O/Ar at φ=1 at 39.1-40.7 bar, modelled IDTs at 40 bar.

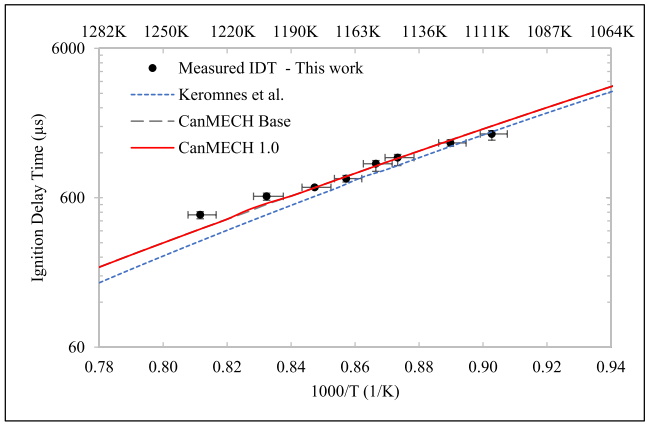

Fig. 5. Measured IDTs for 4%H_2/30%H_2O/15%CO_2/Ar φ=1 at 40.4-41.6 bar, modelled IDTs at 40 bar.

The two CanMECH models have similar predictions, and perfectly overlap with identical RMSREs of 0.192. While all models underestimate IDTs at temperatures higher than 1128 K, CanMECH Base shows improved performance with 29% lower RMSRE than the incumbent. This indicates that CanMECH Base without any parameter tuning is better suited to predict 45% H_2O-laden IDTs.

Figure 5 illustrates measured IDTs for 4%H_2/30%H_2O/15%CO_2/Ar φ=1 at 1108-1232 K and 40.4-41.6 bar, superimposed with modelled IDTs at 40 bar. The two CanMECH models have identical RMSREs (0.097) and perfectly overlap. While CanMECH Base slightly underpredicts IDTs above 1200 K, it outperforms the incumbent model (RMSRE of 0.097 vs. 0.179) which underpredicts most measurements. Modelled IDTs have a higher global activation energy than measurements but CanMECH Base is closer to experiments.

Figure 6 depicts measured IDT results for 4%H_2/45%CO_2/Ar φ=1 at 1226-1133 K and 39.3-43.8 bar, in addition to modelled IDTs at 40 bar. The three models perform similarly with RMSRE of the incumbent slightly lower than CanMECH Base (RMSRE of 0.075 vs. 0.08).

RMSRE values (Table 2) indicate CanMECH Base predicts Shao et al. [16] H_2O- and CO_2-laden IDT data better than the incumbent.

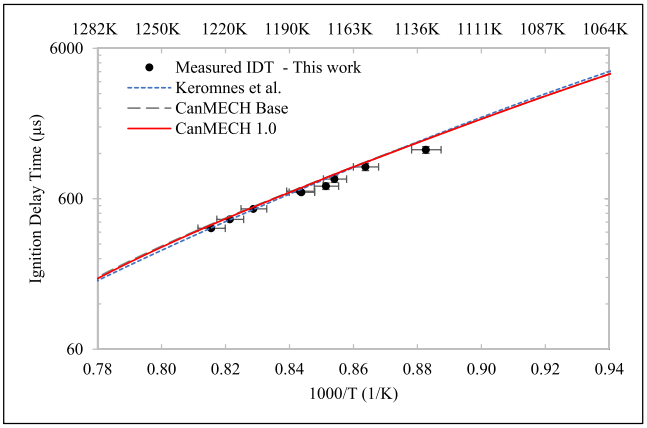

Fig. 6. Measured IDTs 4%H_2/45%CO_2-Ar φ=1 at 39.3-43.8 bar, modelled IDTs at 40 bar.

CanMECH Base outperforms the incumbent for every subset of this data. Shao et al. [16] validation targets involved pressures of 11.4 to 32.9 bar, with bath gases ranging from 4.4-13.4% H_2O/Ar, Ar, N_2, and 10-20%CO_2/Ar.

Performance of the models was also evaluated against 4%H_2/2%O_2/Ar shock tube IDT measurements of Pang et al. [31], at 924-1118 K, 3.42-3.76 bar, and Ninnemann et al. [30] at 960-1131 K, 3.13-5.51 bar. Table 2 RMSRE values indicate that Keromnes et al. mechanism [32] performs significantly better than CanMECH Base, with lower RMSREs by a factor of about three and two relative to the two datasets, respectively. Figures S64 and S65 show that CanMECH Base systematically overpredicts these low-pressure Ar-diluted data.

Dataset 6, from Keromnes et al. [32], involves lean H_2 ignition IDTs in N_2 at 1, 4 and 16 bar. Table 2's RMSREs indicate that the incumbent performs slightly better at pressures of 1 and 16 bar, whereas CanMECH Base improves the predictions at 4 bar. Combined RMSRE of the data for the three pressures show that adoption of CanMECH Base brings about 15% improvement in IDT prediction ability.

Dataset 7, from Keromnes et al. [32], examines H_2-rich mixture IDTs at 1, 4, and 16 bar. Table 2 indicates both CanMECH Base and Keromnes et al. [32] have reasonable performance at the three test pressures. The incumbent has superior performance to CanMECH Base at all three pressure points, with overall RMSRE of CanMECH Base being 14% higher relative to Keromnes et al. [32].

Dataset 8, from Keromnes et al. [32], tests the CO submechanism for fuel-lean H_2/CO mixture at 16 bar. Table 2 indicates that CanMECH Base performs better than the incumbent, with a 2.6% lower RMSRE.

Dataset 9, from Keromnes et al. [32], involves stoichiometric H_2/CO mixture IDTs at 1, 4, and 16 bar. Table 2 illustrates that while CanMECH Base performs better at 4 bar, Keromnes et al. performs better at 1 and 16 bar. Combined RMSREs for the three pressures indicate that the incumbent outperforms CanMECH Base with an overall RMSRE of 0.216 vs. 0.251.

The above examinations of RMSREs demonstrate that CanMECH Base performs better for all H_2O- and CO_2- laden H_2 IDT validation targets of this work, and for high-pressure Ar-diluted experiments (30 and 40 bar). Keromnes et al. model [32] performs better in all low-pressure Ar-diluted experiments. As CanMECH Base consistently overpredicts the IDT for the low-pressure Ar-diluted data of Pang et al. [31], Ninnemann et al. [30] and of the present work, parameter tuning must aim at reducing IDTs under these conditions without negatively impacting high-pressure IDT predictions.

Based on these conclusions, bath-gas-dependent rates involving Ar are likely candidates for parameter tuning. To identify appropriate tuning parameters, pressure- and temperature-dependent IDT sensitivity analyses were conducted. IDT sensitivity analyses involve increasing and decreasing the rate coefficient of each reaction by a factor, "a", in-line with Aul et al. approach [105]. In these analyses, the sensitivity coefficient σ is:

$$\sigma = \frac{\log\left(\frac{\tau'}{\tau''}\right)}{\log\left(\frac{a}{1/a}\right)} \quad (3)$$

where τ' and τ'' are the IDTs calculated with the increased and decreased reaction rate parameter, respectively. A negative sensitivity coefficient means increasing the rate parameter reduces IDTs (increased reactivity), whereas a positive sensitivity coefficient means increasing the rate parameter increases IDTs (decreased reactivity) [105].

Figures 7 and 8 list σ values of rate parameters for 4%H_2/Ar φ=1 at pressures of 2, 4, and 40 bar at 1209 K and 1000 K, respectively. Sensitivities at 2 bar at 1209 K illustrate IDTs decrease by increases in R1 rate, and to lesser extents by the rates of R2, R3 and R10, whereas, IDTs increase with increases in R9 Ar-specific low-pressure-limit rate (R9-A0-Ar). At 1000 K, Fig. 8 shows that at pressures lower than 4 bar, IDTs are sensitive to the following rates, R1, R9-A0-Ar and R9's baseN_2 low-pressure-limit (R9-A0-baseN_2) rates, R2, R17: H_2O_2+H=H_2+HO_2, and R11: HO_2+H=OH+OH. R1 and R9-A0-Ar impacts are larger than others, rendering these more suitable for tuning. Combining the results of 2 and 3.7 bar IDT sensitivities at 1000 and 1209 K, R3, R17, R10, R11, and R9-A0-baseN_2 rates are excluded as potential tuning parameters, considering their small impact either at 1000 K or 1209 K at 2 bar. Thus, the revised list of candidates reduces to R1, R9-Ar-A0 and R2.

Sensitivity results of Fig. 7 show that at 40 bar and 1209 K, relevant to the experimental IDT conditions of this work, R9 and R17 have an increased impact on IDTs. Sensitivity coefficient of R10 switches sign and increases IDTs at 40 bar. In addition to R1, other reactions with significant negative sensitivity coefficient include R17, R11, and Ar-specific low-pressure-limit rate of R15: H_2O_2(+M)=OH+OH(+M). Figures 1 and 3 show that the models overpredict measured IDTs at both 2 and 40 bar near 1209 K. As such, R10 is unlikely to be suitable for tuning as it increases IDTs at 2 bar but decreases them at 40 bar. R17, R11 and R15 are also less likely candidates as they only affect the high-pressure IDTs (at 1209 K). This limits candidate tuning parameters to R1, R9-Ar-A0, and to a lesser extent R2.

The conclusions drawn based on 40 bar IDT-sensitivity analysis results at 1209 K were confirmed at other temperatures relevant to this study. Temperature-dependent IDT-sensitivity analyses conducted at 40 bar indicated that the sensitivities of target tuning parameters do not change sign over the temperature range explored here, see Fig. S67.

In contrast to Ar-diluted IDTs, to improve the fit of 45% and 30% H_2O-laden experimental data, an increase in CanMECH Base's IDTs is needed at temperatures above 1128 and 1200 K, respectively (see Figs. 4 and 5). Additionally, Fig. 6 indicates that the CO_2-laden modelled IDTs need to remain unperturbed.

Figure 9 depicts IDT-sensitive parameters at 2 and 40 bar for 45%H_2O-laden data at 1222 K. At 40 bar, R17, R3, R1, R19, R14 and R15, are the reactions that decrease IDTs, sorted from the most to the least impactful. Conversely, R13, R9, and R10 increase IDTs. In contrast to the Ar-diluted IDT sensitivities, dominant effect of R9-A0-Ar is replaced by the H_2O-specific low-pressure-limit rate (R9-A0-H_2O). This reaffirms suitability of R9-A0-Ar for tuning, as it does not affect the fit of 45% H_2O-laden data. As R17, R3, R2, and R1 decrease IDTs of the H_2O-laden experiments, increasing their rate, required by Ar-diluted experiments, would adversely impact the fit of H_2O-laden data. Hence, R17, R3, R2, and R1 are unlikely candidates for tuning. Due to the small effect of R14 and R15 on

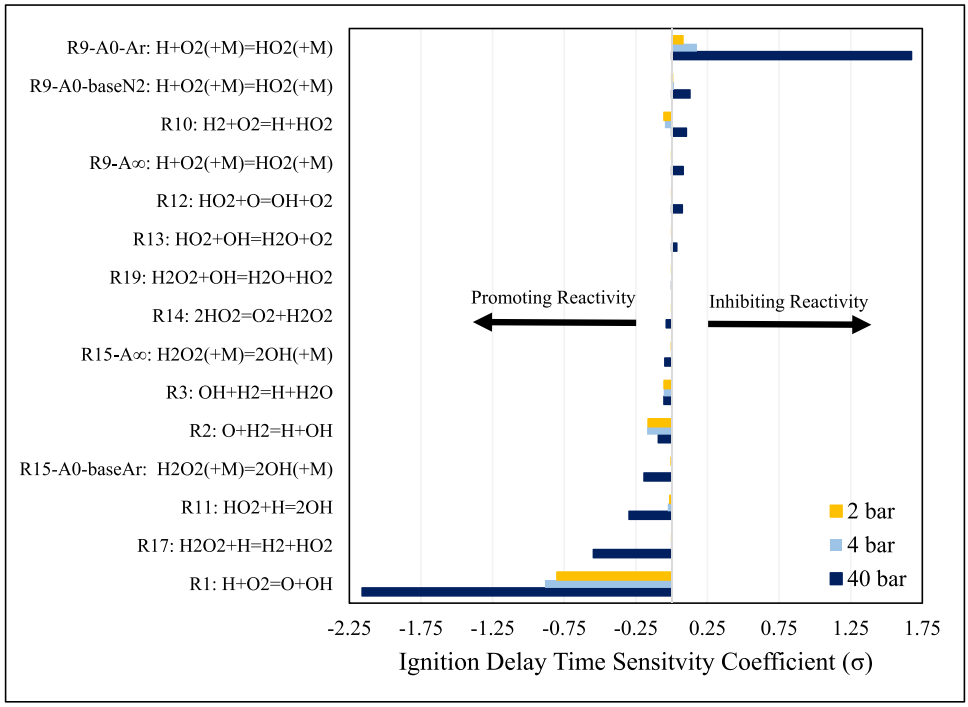

Fig. 7. IDT-sensitive reaction rate parameters (max|σ|≥0.02) for 4%H_2/Ar φ=1 at 1209 K and pressures of 2, 4 and 40 bar.

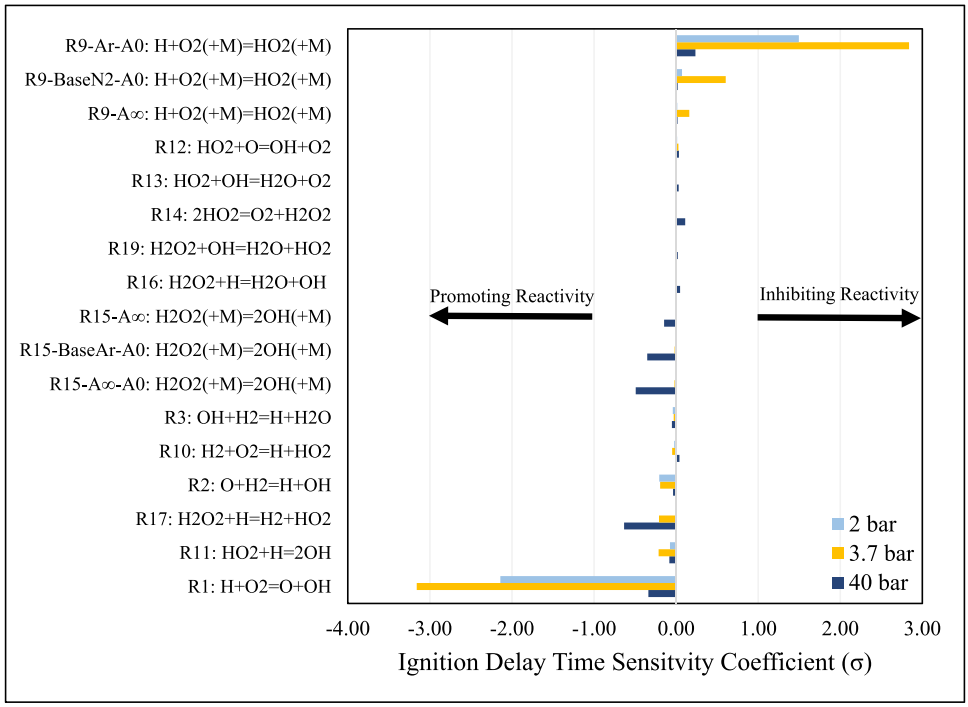

Fig. 8. IDT-sensitive reaction rate parameters (max|σ|≥0.02) for 4%H_2/Ar φ=1 at 1000 K and pressures of 2, 3.7 and 40 bar.

IDTs of validation dataset 4, they are also not considered for tuning. This leaves R9-A0-Ar as the remaining candidate for parameter tuning. These conclusions drawn based on sensitivities at 1222 K and 40 bar were confirmed to be valid through temperature-dependent IDT sensitivity analyses at 40 bar, see Fig. S68.

Similar pressure- and temperature-dependent IDT sensitivity analyses were also conducted for the same reactive mixture in 30%H_2O/15%CO_2/Ar bath, see Fig. S69 and Fig. S70, and in 45%CO_2/Ar bath, see Fig. S71 and Fig. S72, which confirmed appropriateness of the target tuning reaction R9-A0-Ar.

Based on the above sensitivity analyses, the only reaction rate that improves the fit of the analyzed datasets is R9: $H+O_2(+M)=HO_2(+M)$ Ar-specific low-pressure-limit rate. This parameter has little effect on the H_2O- and CO_2-laden IDT data of this work. Finally, because of the reasonable fit of the overall activation energies in Figs. 1,2, Fig. S64 and Fig. S65, the choice of pre-

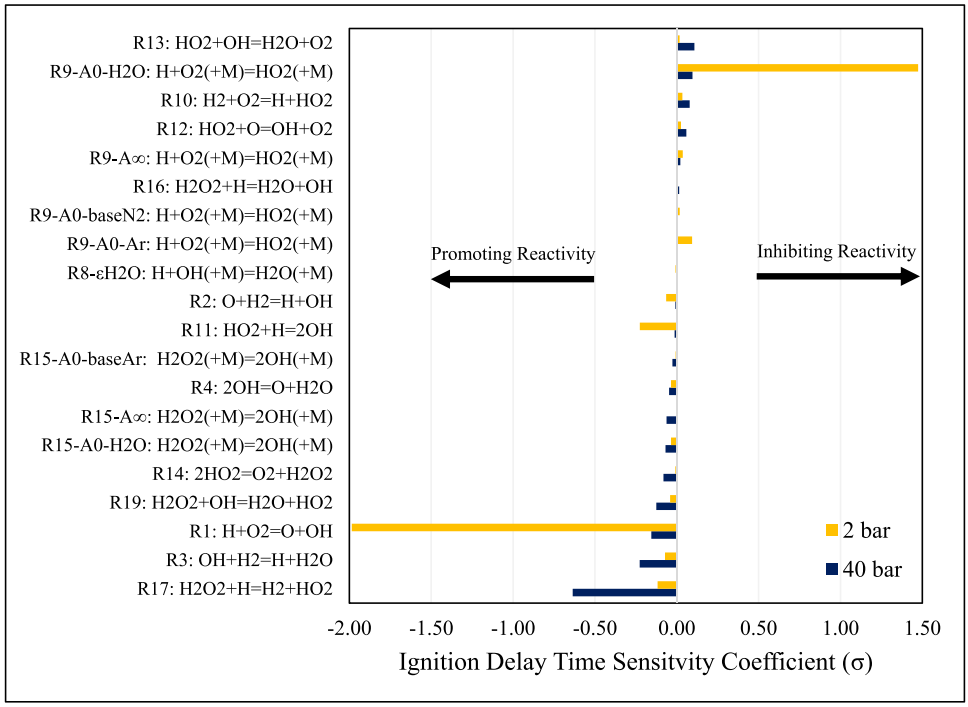

Fig. 9. IDT-sensitive reaction rate parameters ($\sigma \geq 0.02$) for 4%H_2/45%H_2O/Ar φ=1 at 1222 K and pressures of 2 and 40 bar.

exponential factor, A, as the tuning parameter is deemed appropriate. To determine the extent of tuning required, a parametric study was conducted on the A-factor of R9 Ar-specific low-pressure-limit rate (see Table S6). The source of this rate, Shao et al. 2019 study [16], reported a maximum uncertainty of ±12%; hence, the extent of adjustment was kept below this limit. As sensitivity analyses indicated that increasing this reaction rate increases IDTs at low and high pressures, rate multipliers with values between 1 and 0.88 (-12% adjustment) were examined, and the lowest value of 0.88 produced the lowest overall RMSRE (see Table S6).

CanMECH Base with only one tuned parameter, the Ar-specific low-pressure-limit rate of R9 reduced by 12%, constitutes CanMECH 1.0 which is the proposed H_2/CO mechanism in this work.

RMSRE values in Table 2 show that the minimally tuned mechanism, CanMECH 1.0, outperforms the incumbent Keromnes et al. mechanism for the majority of datasets. CanMECH 1.0 also exhibits the lowest overall RMSRE, which brings about a 14% improvement relative to the incumbent model [32].

RMSRE values for ~2.25 bar Ar-diluted experimental IDTs of this work show that while parameter tuning reduced CanMECH 1.0's RMSRE by 4% relative to CanMECH Base, Keromnes et al. [32] still outperformed CanMECH 1.0, indicated by an RPRMSRE of +6%. Re-examination of Fig. 1 shows that the parameter tuning narrowed the error gap relative to the experimental results. While further reduction of R9 Ar-specific low-pressure-limit would have reduced the deviation, the 12% prescribed uncertainty limit by Shao et al. [16] precludes applying a rate multiplier lower than 0.88 (-12% adjustment). Better performance of Keromnes et al. [32] is likely due to its lower pre-exponential factor for R9 Ar-specific low-pressure-limit rate relative to CanMECH 1.0 (see Fig. S73). For the ~2.5 bar CO_2-diluted data of this work, the RMSRE values reduced with smaller values of the rate multiplier. Examination of Fig. 2 also shows that the parameter tuning has a desirable impact on the modelled IDTs for 4%H_2/45%CO_2/Ar φ=1 at ~2.5 bar. Its impact is also smaller relative to that observed for the low-pressure Ar-diluted experiments. This is due to the increased concentration of CO_2 displacing Ar, which has a five times larger third-body collision efficiency than Ar for R9. Nevertheless, an RPRMSRE of -62% indicates that CanMECH 1.0 has 62% better performance relative to the incumbent for the low-pressure 45%CO_2-laden IDTs. Moreover, RPRMSRE for dataset 1 suggests a 51% reduction in the relative errors.

For the 40-bar Ar-diluted IDTs (dataset 2), CanMECH 1.0 exhibits the lowest RMSRE, and it brings about a 45% improvement relative to the incumbent mechanism.

RMSRE values of Table 2 also suggest that the tuning implemented is inconsequential to the fit of 45% H_2O- and 30%H_2O/15%CO_2-laden experimental data. Figures 4 and 5 show that CanMECH 1.0 provides better estimates of the measured IDTs and their global activation energy relative to the incumbent. This is signified by the RPRMSRE values of -29% and -46% for the 45%H_2O- and 30%H_2O/15%CO_2-laden data. Figures 4 and 5 also show that the implemented parameter adjustment has improved the predicted activation energy relative to CanMECH Base.

Examination of the RMSRE values of the 45%CO_2 experimental IDTs illustrates that the parameter adjustment reduces the RMSRE and further improves the fit. Inferior performance of CanMECH Base is remedied as prediction ability of CanMECH 1.0 matches that of the incumbent (RPRMSRE of 0%). Overall, adoption of CanMECH 1.0 brings about a 33% improvement relative to the incumbent in representing the high-pressure IDT experimental data of this work.

RMSRE values of Table 2 for dataset 3 show that while the tuning improves the fit of H_2O- and 20%CO_2-laden data, it adversely impacts the fit of Ar- and 10%CO_2-diluted experiments. This is expected as Shao et al. [16] optimized R9's Ar low-pressure-limit rate for the best fit of their experimental IDTs. Hence, any tuning of this rate was expected to increase RMSRE of CanMECH 1.0 for Shao et al. [16] dataset. However, RPRMSRE values indicate that CanMECH 1.0 outperforms Keromnes et al. in predicting all but one of Shao et al. [16] validation subset for 3%H_2/1.5%O_2/10%CO_2/Ar. There were only two IDT measurements in this subset, and while an RPRMSRE of +96% is undesirable, CanMECH 1.0 predictions are still within the large error bounds of experimental data (see Fig.

S74). Hence, the seemingly high RPRMSRE is not of concern considering the reported uncertainties of ±39% and ±42% of the measured IDTs [16]. The overall RPRMSRE for the complete IDT validation dataset of Shao et al. [16] exhibits a 37% improvement brought about by CanMECH 1.0 relative to Keromnes et al. model [32].

Table 2 illustrates that the implemented parameter tuning significantly improves the RMSRE values of Pang et al. [31] and Ninnemann et al. [30] data. While Keromnes et al. mechanism [32] performs better for the lower temperature data, both models capture many of the data points within their uncertainties due to the scatter of the experimental data, see Fig. S64 and S65. The improved performance of Keromnes et al. model is attributed to their lower pre-exponential factor of R9 Ar-specific low-pressure-limit rate relative to the reduced rate in CanMECH 1.0. The incumbent has a better performance with an RPRMSRE of 40% and 31%, respectively, for the two datasets. It should also be noted that the reproducibility of the low-temperature IDT experimental results, such as that of Pang et al. [31], as noted by the Ninnemann et al. [30], is highly sensitive to accurate measurements of the dp/dt effect which is not commonly available. Facility-specific average dp/dt of 2 and 2.5%/ms were implemented when reproducing Pang et al. [31] and Ninnemann et al. [30] experimental data, respectively.

Comparison of the RMSRE values of the N_2-diluted validation dataset 6 (Table 2) shows that the parameter tuning is inconsequential as the reactive mixture does not contain any Argon. The RPRMSRE value of -15% indicates that CanMECH 1.0 provides improved IDT predictions relative to the incumbent.

Table 2 illustrates that for the Ar-diluted hydrogen-rich mixture of dataset 7, the parameter tuning improves the model fit at all three pressures of 1, 4 and 16 bar. The combined RPRMSRE indicates that CanMECH 1.0 improves RMSREs by 5% relative to Keromnes et al. mechanism [32].

RMSRE results for the validation dataset 8 indicates that the parameter tuning slightly improves the overall fit for CanMECH 1.0 relative to CanMECH Base. CanMECH 1.0 outperforms the incumbent, signified by an RPRMSRE of -3%.

For dataset 9, Table 2 indicates that while parameter tuning slightly increases the RMSRE at 1 bar for 2.96%H_2/2.96%CO/2.96%O_2/Ar IDTs, the RMSRE reduces for 4 and 16 bar data. Keromnes et al. [32] outperforms CanMECH 1.0 for the 1 bar and to a lesser extent 16 bar data. CanMECH 1.0 brings about an 11% improvement in the RMSRE value for the 4 bar data. Overall, for dataset 9, the RPRMSRE shows that the incumbent has a 5% lower RMSRE than CanMECH 1.0.

8. Conclusions

Novel shock tube IDT measurements were performed for stoichiometric 4% H_2 at pressures of 37-43.8 bar and 2.1-2.7 bar in bath gas of Ar, 45%H_2O/Ar, 30%H_2O/15%CO_2/Ar, and 45%CO_2/Ar. High-pressure tests spanned temperatures of 1084-1242 K, and low-pressure tests spanned 926-1198 K. An H_2/CO combustion mechanism, CanMECH 1.0, was developed, with a focus on pressure-dependent reaction rates and the impact of strong third-body colliders, namely, H_2O and CO_2. The mechanism will serve as a platform for further model developments and improvements focused on such bath gases. Through sensitivity analyses, pre-exponential factor of reaction R9: $H+O_2(+M)=HO_2(+M)$ Ar-specific low-pressure-limit rate was tuned by a factor of 0.88. The model was validated against shock tube IDT data of this work, as well as H_2 and H_2/CO validation datasets from literature. This mechanism performance was also compared to the well-cited Keromnes et al. mechanism [32]. Out of the 26 subsets of validation data examined, CanMECH 1.0 outperformed Keromnes et al. mechanism [32] for 16 datasets, and had an identical performance for another two. Considering all validation datasets, CanMECH 1.0 brought about a 14% improvement relative to Keromnes et al. mechanism [32]. Of particular importance, CanMECH 1.0 significantly outperformed Keromnes et al. mechanism [32] in predicting shock tube IDTs for H_2O- and CO_2-laden reactive mixtures as well as all IDT data at pressures of 17-43.8 bar.

Declaration of Competing Interest

The authors declare that they have no known competing financial interests or personal relationships that could have appeared to influence the work reported in this paper.

Acknowledgments

This work was supported by Natural Resources Canada, Office of Energy Research and Development's (OERD) Program of Energy Research and Development (PERD), and by the Office of Sponsored Research (OSR) at King Abdullah University of Science and Technology (KAUST).

Supplementary materials

Supplementary material associated with this article can be found, in the online version, at doi:10.1016/j.combustflame.2022.112498.

References

[1] International Energy Agency, World Energy Outlook 2020Executive Summary, International Energy Agency, Paris, France, 2020.
[2] A. Beigzadeh, A. Shafeen, M. Abbassi, C. Salvador, K.E. Zanganeh, Optimized multi-pollutant control in oxy-fuel combustion systems using CO2 capture and compression process, Energy Procedia 63 (2014) 8134–8143.
[3] N.T. Weiland, C.W. White, Performance and Cost Assessment of A Natural Gas-Fueled Direct sCO2 Power Plant, National Energy Technology Laboratory, Pittsburgh, USA, 2019.
[4] K. Zanganeh, A. Shafeen, C. Salvador, A. Beigzadeh, G2 Technology for production of power, water or steam and pipeline-ready pressurized CO2, 5th Oxyfuel Combustion Research Network Meeting, Wuhan, 2015.
[5] K. Brun, P. Friedman, R. Dennis, Fundamentals and Applications of Supercritical Carbon Dioxide (SCO2) Based Power Cycles, Elsevier - WOODHEAD PUBLISHING, Duxford, U.K, 2017.
[6] O. Pryor, S. Barak, J. Lopez, E. Ninnemann, B. Koroglu, L. Nash, S.S. Vasu, High pressure shock tube ignition delay time measurements during oxy-methane combustion with high levels of CO2 dilution, J. Energy Resour. Technol. 139 (4) (2017) 042208-1-6.
[7] O. Pryor, S. Barak, B. Koroglu, E. Ninnemann, S.S. Vasu, Measurements and interpretation of shock tube ignition delay times in highly CO2 diluted mixtures using multiple diagnostics, Combust. Flame 180 (2017) 63–76.
[8] B. Koroglu, O.M. Pryor, J. Lopez, L. Nash, S.S. Vasu, Shock tube ignition delay times and methane time-histories measurements during excess CO2 diluted oxy-methane, Combust. Flame 164 (2016) 152–163.
[9] J. Shao, R. Choudhary, D.F. Davidson, R.K. Hanson, S. Barak, S. Vasu, Ignition delay times of methane and hydrogen highly diluted in carbon dioxide at high pressures up to 300 atm, Proc. Combust. Inst. 37 (2019) 4555–4562.
[10] S. Barak, E. Ninnemann, S. Neupane, F. Barnes, J. Kapat, S. Vasu, High-pressure oxy-syngas ignition delay times with CO2 dilution: shock tube measurements and comparison of the performance of kinetic mechanisms, J. Eng. Gas Turbines Power 141 (2019) 021011-1-021011-7.
[11] A.N. Mazas, D.A. Lacoste, T. Schuller, Experimental and numerical investigation on the laminar flame speed of CH4/O2 mixtures diluted with CO2 and H2O, Proceedings of ASME Turbo Expo 2010: Power for Land, Sea and Air, Glasgow (2010).
[12] N. Donohoe, K.A. Heufer, C.J. Aul, E.L. Petersen, G. Bourque, R. Gordon, H.J. Curran, Influence of steam dilution on the ignition of hydrogen, syngas and natural gas blends at elevated pressures, Combust. Flame 162 (1) (2015) 1126–1135.
[13] T. Turanyi, A.S. Tomlin, Analysis of Kinetic Reaction Mechanisms, Springer, Heidelberg, Germany, 2014.
[14] S.J. Klippenstein, From theoretical reaction dynamics to chemical modeling of combustion, Proc. Combust. Inst. 36 (1) (2017) 77–111.
[15] D.L. Baulch, C.T. Bowman, C.J. Cobos, R.A. Cox, T. Just, J.A. Kerr, M.J. Pilling, D. Stocker, J. Troe, W. Tsang, R.W. Walker, Evaluated kinetic data for combustion modeling: supplement II, J. Phys. Chem. Ref. Data 34 (3) (2005) 757–1397.

[16] J. Shao, R. Choudhary, A. Susa, D.F. Davidson, R.K. Hanson, Shock tube study of the rate constants for H+O2+M ->HO2+M(M=Ar, H2O, CO2, N2) at elevated pressures, Proc. Combust. Inst. 37 (2019) 145–152.
[17] A NSYS Chemkin-Pro 2019 R3, ANSYS, Penssylvania, 2019.
[18] S.M. Burke, J.M. Simmie, H.J. Curran, Critical evaluation of thermochemical properties of C1-C4 species: updated group-contributions to estimate thermochemical properties, J. Phys. Chem. Ref. Data 44 (1) (2015) 013101-1-28.
[19] National Institute of Standards and Technology, NIST Chemistry Webbok, SRD 69," U.S. Secretary of Commerce on behalf of the United States of America. <https://webbook.nist.gov/chemistry/fluid/>. [Accessed 6 January 2021].
[20] B. Ruscic, Active Thermochemical Tables (ATcT), US Argonne National Laboratory, 2020 <Available: http://atct.anl.gov/ >[Accessed 24 November 2020].
[21] C.-W. Zhou, Y. Li, U. Burke, C. Banyon, K.P. Somers, S. Ding, S. Khan, J.W. Hargis, T. Sikes, O. Mathieu, E.L. Petersen, M. AlAbbad, A. Farooq, Y. Pan, Y. Zhang, Z. Huang, J. Lopez, Z. Loparo, S.S. Vasu, H.J. Curran, An experimental and chemical kinetic modeling study of 1,3-butadiene combustion: ignition delay time and laminar flame speed measurements, Combust. Flame 197 (2018) 423–438.
[22] A. Burcat, B. Ruscic, Third Millennium Ideal Gas and Condensed Phase Thermochemical Database for Combustion with Updates from Active Thermochemical Table, U.S. Department of Energy's Argonne National Laboratory, Argonne, USA, 2005.
[23] C.W. Gao, J.W. Allen, W.H. Green, R.H. West, Reaction mechanism generator: automatic construction of chemical kinetic mechanisms, Comput. Physics Commun. 203 (2016) 212–225.
[24] J.W. Allen, F. Goldsmith, W.H. Green, Automatic estimation of pressure-dependent rate coefficients, Phys. Chem. Chem. Phys. 14 (3) (2011) 1131–1155.
[25] M.P. Burke, M. Chaos, Y. Ju, F.L. Dryer, S.J. Klippenstein, Comprehensive H2/O2 kinetic model for high-pressure combustion, Int. J. Chem. Kinet. 44 (7) (2012) 444–474.
[26] M.P. Burke, R. Song, Evaluating mixture rules for multi-component pressure dependence: H+O2(+M)=HO2(+M), Proc. Combust. Inst. 36 (1) (2017) 245–253.
[27] A.A. Konnov, Yet another kinetic mechanism for hydrogen combustion, Combust. Flame 203 (2019) 14–22.
[28] J. Urzay, N. Kseib, D.F. Davidson, G. Iaccarino, R.K. Hanson, Uncertainty-quantification analysis of the effects of residual impurities on hydrogen-oxygen in shock tubes, Combust. Flame 161 (2014) 1–15.
[29] C.R. Mulvihill, E.L. Petersen, Concerning shock-tube ignition delay times: an experimental investigation of impurities in the H2/O2 system and beyond, Proc. Combust. Inst. 37 (1) (2019) 259–266.
[30] E. Ninnemann, B. Koroglu, O. Pryor, S. Barak, L. Nash, Z. Loparo, J. Sosa, K. Ahmed, S. Vasu, New insights into the shock tube ignition of H2/O2 at low to moderate temperatures using high-speed end-wall imaging, Combust. Flame 187 (2018) 11–21.
[31] G.A. Pang, D.F. Davidson, Experimental study and modeling of shock tube ignition delay times for hydrogen–oxygen–argon mixtures at low temperatures, Proc. Combust. Inst. 32 (1) (2009) 181–188.
[32] A. Keromnes, W.K. Metcalfe, K.A. Heufer, N. Donohoe, A.K. Das, C.-J. Sung, J. Herzler, C. Naumann, P. Griebel, O. Mathieu, M.C. Krejci, E.L. Petersen, W.J. Pitz, H.J. Curran, An experimental and detailed chemical kinetic modeling study of hydrogen and syngas mixture oxidation at elevated pressures, Combust. Flame 160 (2013) 995–1011.
[33] E.L. Petersen, R.K. Hanson, Measurement of reflected-shock bifurcation over a wide range of gas composition and pressure, Shock Waves 15 (2006) 333–340.
[34] J.W. Hargis, E.L. Petersen, Methane ignition in a shock tube with high levels of CO2 dilution: consideration of the reflected-shock bifurcation, Energy Fuels 29 (2015) 7712–7726.
[35] M. Figueroa-Labastida, M.B. Luong, J. Badra, H.G. Im, A. Farooq, Experimental and computational studies of methanol and ethanol preignition behind reflected shock waves, Combust. Flame 234 (2021) 111621.
[36] K.P. Grogan, M. Ihme, Regimes describing shock boundary layer interaction and ignition in shock tubes, Proc. Combust Inst. 36 (2017) 2927–2935.
[37] T. Varga, T. Nagy, C. Olm, I.G. Zsely, R. Palvolgyi, E. Valko, G. Vincze, M. Cserhati, H.J. Curran, T. Turanyi, Optimization of a hydrogen combustion mechanism using both direct and indirect measurements, Proc. Combust. Inst. 35 (2015) 589–596.
[38] C. Olm, I.G. Zsely, T. Varga, H.J. Curran, T. Turanyi, Comparison of the performance of several recent syngas combustion mechanisms, Combust. Flame 162 (2015) 1793–1812.
[39] V.A. Alekseev, M. Christensen, A.A. Konnov, The effect of temperature on the adiabatic burning velocities of diluted hydrogen flames: a kinetic study using an updated mechanism, Combust. Flame 162 (2015) 1884–1898.
[40] G.P. Smith, Y. Tao, H. Wang, Foundational Fuel Chemistry Model Version 1.0 (FFCM-1), Stanford University, 2016 http://web.stanford.edu/group/haiwanglab/FFCM1/pages/trialrates.html [Accessed 2017].
[41] Z. Hong, D.F. Davidson, R.K. Hanson, An improved H2/O2 mechanism based on recent shock tube/laser absorption measurements, Combust. Flame 158 (4) (2011) 633–644.
[42] Z. Hong, D.F. Davidson, A new shock tube study of the H+O2->OH+O reaction rate using tunable diode laser absortion of H2O near 2.5 m, Proc. Combust. Inst. 33 (2011) 309–316.
[43] J.W. Sutherland, P.M. Patterson, R.B. Klemm, Rate constants for the reaction, O(3P)+H2O=OH+OH, over the temperature range 1053 to 2033 K using two direct techniques, Symp. (Int.) Combust. 23 (1990) 51–57.
[44] K.-Y. Lam, D.F. Davidson, R.K. Hanson, A shock tube study of H2+OH→H2O+H using OH laser absorption, Int. J. Chem. Kinet. 45 (6) (2013) 363–373.
[45] J.V. Michael, J.W. Sutherland, Rate constant for the reaction of H with H2O and OH with H2 by the flash photolysis-shock tube technique over the temperature range 1246-2297K, J. Phys. Chem. 92 (13) (1988) 3853–3857.
[46] G. Altinay, G.R. Macdonald, Determination of the rate constant for the OH(X2Π) + OH(X2Π) →H2O + O(3P) reaction over the temperature range 295 to 701 K, J. Phys. Chem. A 118 (1) (2014) 38–54.
[47] M.S. Wooldrige, R.K. Hanson, C.T. Bowman, A shock tube study of the OH + OH ->H2O + O Reaction, Int. J. Chem. Kinet. 26 (4) (1994) 389–401.
[48] N. Cohen, Chemical kinetic data sheets for high-temperature chemical reactions, J. Phys. Chem. Ref. Data 12 (3) (1983) 531–590.
[49] W. Tsang, R.F. Hampson, Chemical kinetic data base for combustion chemistry. Part I. methane and related compounds, J. Phys. Chem. Ref. Data 15 (3) (1986) 1087–1222.
[50] W.C. Gardiner, Combustion Chemistry, Springer-Verlag, New York, USA, 1984.
[51] V. Naudent, J. Sandra, C.E. Paillard, A high temperature chemical kinetics study of the reaction: OH+Ar=H+O+Ar by atomic resonance absorption spectrophotometry, Combust. Sci. Technol. 164 (2001) 113–128.
[52] S.R. Sellevåg, Y. Georgievskii, J.A. Miller, Kinetics of the gas-phase recombination reaction of hydroxyl radicals to form hydrogen peroxide, J. Phys. Chem. A 113 (16) (2009) 4457–4467.
[53] J. Li, A. Kazakov, F.L. Dryer, An updated comprehensive kinetic model of hydrogen combustion, Int. J. Chem. Kinet. 36 (10) (2004) 566–575.
[54] N.K. Srinivasan, J.V. Michael, The thermal decomposition of water, Int. J. Chem. Kinet. 38 (3) (2006) 211–219.
[55] J. Troe, Detailed modeling of the temperature and pressure dependence of the reaction H+O2 (+M)→HO2 (+M), Proc. Combust. Inst. 28 (2) (2000) 1463–1469.
[56] R.W. Bates, D.M. Golden, R.K. Hanson, C.T. Bowman, Experimental study and modeling of the reaction H+O2+M->HO2+M (M=Ar, N2, H2O) at elevated pressures and temperatures between 1050 and 1250 K, Phys. Chem. Chem. Phys. 3 (12) (2001) 2337–2342.
[57] R.X. Fernandes, K. Luther, J. Troe, V.G. Ushakov, Experimental and modelling study of the recombination reaction H+O 2 (+M) - HO2 (+M) between 300 and 900 K, 1.5 and 950 bar, and in the bath gases M = He, Ar, and N2, Physc. Chem. Chem. Phys. 10 (29) (2008) 4313–4321.
[58] S. M-C J.V. Michael, J.W. Sutherland, J.J. Carroll, A.F. Wager, Rate constants for H + O2 + M → HO2 + M in seven bath gases, J. Phys. Chem. A. 106 (21) (2002) 5297–5313.
[59] G. P. Smith, D. M. Golden, M. Frenklach, N. W. Moriarty, B. Eiteneer, M. Goldenberg, C. T. Bowman, H. R. K. S. Song, W. C. J. Gardiner, V. Lissianski and Z. Qin, GRI-MECH 3.0, http://www.me.berkeley.edu/gri_mech/. [Accessed 20 June 2017].
[60] V.J. Michael, J.W. Sutherland, L.B. Harding, A.F. Wagner, Initiation in H2/O2: rate constants for H2 + O2 → H + HO2 at high temperature, Proc. Combust. Inst. 28 (2) (2000) 1471–1478.
[61] M.A. Mueller, R.A. Yetter, F.L. Dryer, Flow reactor studies and kinetic modeling of the H2/O2/NOX and CO/H2O/O2/NOX reactions, Int. J. Chem. Kinet. 31 (10) (1999) 705–724.
[62] D.L. Baulch, C.J. Cobos, R.A. Cox, C. Esser, P. Frank, T. Just, J.A. Kerr, M.J. Pilling, J. Troe, R.W. Walker, J. Warrantz, Evaluated kinetic data for combustion modelling, J. Phys. Chem. Ref. Data 21 (3) (1992) 411–734.
[63] A. Fernández-Ramos, A.J.C. Varandas, A VTST study of the H + O3 and O + HO2 reactions using a six-dimensional DMBE potential energy surface for ground state HO3, J. Phys. Chem. A 106 (16) (2002) 4077–4083.
[64] Z. Hong, K.-Y. Lam, R. Sur, S. Wang, D.F. Davidson, R.K. Hanson, On the rate constants of OH+HO2 and HO2+HO2: a comprehensive study of H2O2 thermal decomposition using multi-species laser absorption, Proc. Combust. Inst. 34 (1) (2013) 565–571.
[65] L.F. Keyser, Kinetics of the reaction OH+HO2->H2O+O2 from 254 to 382 K, J. Phys. Chem. 92 (1988) 1193–1200.
[66] C. Kappel, K. Luther, J. Troe, Shock wave study of the unimolecular dissociation of H2O2 in its falloff range and of its secondary reactions, Phys. Chem. Chem. Phys. 4 (18) (2002) 4392–4398.
[67] H. Hippler, J. Troe, J. Willner, Shock wave study of the reaction HO2+HO2→H2O2+O2: confirmation of a rate constant minimum near 700 K, J. Chem. Phys. 93 (3) (1990) 1755–1760.
[68] J. Troe, The thermal dissociation/recombination reaction of hydrogen peroxide H2O2(+M)<=>2OH(+M) III. Analysis and representation of the temperature and pressure dependence over wide ranges, Combust. Flame 158 (4) (2011) 594–601.
[69] Z. Hong, R.D. Cook, D.F. Davidson, R.K. Hanson, A shock tube study of OH+ H2O2→ H2O+ HO2 and H2O2+ M→ 2OH+ M using laser absorption of H2O and OH, J. Phys. Chem. A 114 (18) (2010) 5718–5727.
[70] Z. Hong, A. Farooq, E.A. Barbour, D.F. Davidson, R.K. Hanson, Hydrogen peroxide decomposition rate: a shock tube study using tunable laser absorption of H2O near 2.5 μm, J. Phys. Chem. A 113 (46) (2009) 12919–12925.
[71] R. Zellner, F. Ewig, R. Paschke, G. Wagner, Pressure and temperature dependence of the gas-phase recombination of hydroxyl radicals, J. Phys. Chem. 92 (14) (1988) 4184–4190.
[72] R. Forster, M. Frost, D. Fulle, H. Hamann, H. Hippler, A. Schlepegrell, J. Troe, High pressure range of the addition of HO to HO, NO, NO2, and CO. I. Saturated laser induced fluorescence measurements at 298 K, J. Chem. Phys. 103 (1995) 2949–2958.

[73] B.A. Ellingson, D.P. Theis, O. Tishchenko, J. Zheng, D.G. Truhlar, Reactions of hydrogen atom with hydrogen peroxide, J. Phys. Chem. A 111 (51) (2007) 13554–13566.
[74] J. Li, Z. Zhao, A. Kazakov, M. Chaos, F.L. Dryer, J.J. Scire JR., A comprehensive kinetic mechanism for CO, CH2O, and CH3OH combustion, Int. J. Chem. Kinet. 39 (3) (2007) 109–136.
[75] K. S. J H. Hashemi, J.M. Christensen, S. Gersen, H. Levinsky, P. Glarborg, High--pressure oxidation of methane, Combust. Flame 172 (2016) 349–364.
[76] J. Troe, Thermal dissociation and recombination of polyatomic molecules, Symp. (Int.) Combust. 5 (1) (1975) 667–680.
[77] P.R. Westmoreland, J.B. Howard, J.P. Longwell, A.M. Dean, Prediction of rate constants for combustion and pyrolysis reactions by bimolecular QRRK, AIChE 32 (12) (1986) 1971–1979.
[78] A.V. Joshi, H. Wang, Master equation modeling of wide range temperature and pressure dependence of CO + OH → products, Int. J. Chem. Kinet. 38 (1) (2006) 57–73.
[79] J.P. Senosiain, S.J. Klippenstein, J.A. Miller, A complete statistica analysis of the reaction between OH and CO, Proc. Combust. Inst. 30 (2005) 945–953.
[80] X. You, H. Wang, E. Goos, C.-J. Sung, S.J. Klippenstein, Reaction kinetics of CO + HO(2) –>products: ab initio transition state theory study with master equation modeling, J. Phys. Chem. A 111 (19) (2007) 4031–4042.
[81] X. Yang, T. Tan, P. Dievart, E.A. Carter, Y. Ju, Theoretial assessment on reaction kinetics HCO and CH2OH unimolecular decomposition, 8th US Nat. Combust. Meeting 2 (2013) 1732–1740.
[82] G. Friedrichs, J.T. Herbon, D.F. Davidson, R.K. Hanson, Quantitative detection of HCO behind shock waves: the thermal decomposition of HCO, Phys. Chem Chem. Phys. 4 (2002) 5778–5788.
[83] H. Hashemi, J.G. Jacobsen, C.T. Rasmussen, J.M. Christensen, P. Glarborg, S. Gersen, M.v. Essen, H.B. Levinsky, S.J. Klippenstein, High-pressure oxidation of ethane, Combust. Flame 182 (2017) 150–166.
[84] N. Faßheber, G. Friedrichs, P. Marshall, P. Glarborg, Glyoxal oxidation mechanism: implications for the reactions HCO + O2 and OCHCHO + HO2, J. Phys. Chem. A 119 (28) (2015) 7305–7315.
[85] R.S. Timonen, E. Ratajczak, D. Gutman, Kinetics of the reactions of the formyl radical with oxygen, nitrogen dioxide, chlorine, and bromine, J. Phys. Chem. 92 (3) (1988) 651–655.
[86] R.S. Timonen, E. Ratajczak, D. Gutman, Kinetics of the reaction between formyl radicals and atomic hydrogen, J. Phys. Chem. 91 (3) (1987) 692–694.
[87] M. Sangwan, L.N. Krasnoperov, Disproportionation channel of self-reaction of hydroxyl radical, OH+OH →H2O+O, studied by time-resolved oxygen atom trapping, J. Phys. Chem. A 116 (48) (2012) 11817–11822.
[88] M. Sangwan, E.N. Chesnokov, L.N. Krasnoperov, Reaction OH + OH studied over the 298-834 K temperature and 1-100 bar pressure ranges, J. Phys. Chem. A 116 (24) (2012) 6282–6294.
[89] Y. Bedjanian, G.Le Bras, G. Poulet, Kinetic study of OH+OH and OD+OD reactions, J. Phys. Chem. A 103 (35) (1999) 7017–7025.
[90] T.L. Nguyen, J.F. Stanton, Ab initio thermal rate calculations of HO + HO = O(3P) + H2O reaction and isotopologues, J. Phys. Chem. A 117 (13) (2013) 2678–2686.
[91] S.R. Sellevåg, Y. Georgievskii, J.A. Miller, The temperature and pressure dependence of the reactions H + O2 (+M)→HO2 (+M) and H + OH (+M)→H2O(+M), J. Phys. Chem. A 112 (23) (2008) 5085–5095.
[92] J. Hahn, L. Krasnoperov, K. Luther, J. Troe, Pressure dependence of the reaction H + O2(+Ar) → HO2(+Ar) in the range 1–900 bar and 300–700 K, Phys. Chem. Chem. Phys. 6 (9) (2004) 1997–1999.
[93] I. Janik, D.M. Bartels, T.W. Marin, C.D. Jonah, Reaction of O2 with the hydrogen atom in water up to 350°C, J. Phys. Chem. A 111 (1) (2007) 79–88.
[94] L.B. Harding, S.J. Klippenstein, H. Lischka, R. Shepard, Comparison of multireference configuration interaction potential energy surfaces for H + O2 → HO2: the effect of internal contraction, Theor. Chem. Acc. 133 (2014) 1429.
[95] M.P. Burke, S.J. Klippenstein, L.B. Harding, A quantitative explanation for the apparent anomalous temperature dependence of OH+HO2=H2O+O2 through multi-scale modeling, Proc. Combust. Inst. 34 (1) (2013) 547–555.
[96] J. Troe, Ultravioletttspektrum und Reaktionen des HO2-Radikals im thermischen Zerfall von H2O2, Berichte der Bunsengesellschaft für physikalische Chemie 73 (10) (1969) 946–952.
[97] M.B. SAJID, E. ES-SEBBAR, T. JAVED, C. FITTSCHEN, A. FAROOQ, Measurement of the rate of hydrogen peroxide thermal decomposition in a shock tube using quantum cascade laser absorption near 7.7 µm, Int. J. Chem. Kinet. 46 (5) (2014) 275–284.
[98] X. Lu, Q. Meng, B. Fu, D.H. Zhang, Rate coefficients of the H + H2O2 → H2 +HO2 reaction on an accurate fundamental invariant-neural network potential energy surface, J. Chem. Phys. 149 (2018) 174303-1-7.
[99] A.A. Konnov, Remaining uncertainties in the kinetic mechanism of hydrogen combustion, Combust. Flame 152 (4) (2008) 507–528.
[100] A.W. Jasper, R. Dawes, Non-born–oppenheimer molecular dynamics of the spin-forbidden reaction O(3P) + CO(X 1Σ+) → CO2(X˜Σg+1), J. Chem. Phys. 139 (2013) 154313-1-13.
[101] W.K. Metcalfe, S.M. Burke, S.S. Ahmed, H.J. Curran, A hierarchical and comparative kinetic modeling study of C1-C2 hydrocarbon and oxygenated fuels, Int. J. Chem. Kinet. 45 (10) (2013) 638–675.
[102] M. Alabbad, Y. Li, K. AlJohani, G. Kenny, K. Hakimov, M. Al-lehaibi, A.-H. Emwas, P. Meier, J. Badra, H. Curran, A. Farooq, Ignition delay time measurements of diesel and gasoline blends, Combust. Flame 222 (2020) 460–475.
[103] J. Badra, A.E. Elwardany, F. Khaled, S.S. Vasu, A. Farooq, A shock tube and laser absorption study of ignition delay times and OH reaction rates of Ketones: 2-butanone and 3-buten-2one, Combust. Flame 161 (2014) 725–734.
[104] M.F. Campbell, Studies of Biodiesel Surrogates Using Novel Shock Tube Techniques, Stanford University, Stanford, USA, 2014.
[105] C.J. Aul, W.K. Metcalfe, S.M. Burke, H.J. Curran, E.L. Petersen, Ignition and kinetic modeling of methane and ethane fuel blends with oxygen: a design of experiments approach, Combust. Flame. 160 (7) (2013) 1153–1167.

Update

Combustion and Flame

Volume 266, Issue , August 2024, Page

DOI: https://doi.org/10.1016/j.combustflame.2024.113520

Combustion and Flame 266 (2024) 113520

Contents lists available at ScienceDirect

Combustion and Flame

journal homepage: www.sciencedirect.com/journal/combustion-and-flame

Corrigendum to "Reaction kinetics for high pressure hydrogen oxy-combustion in the presence of high levels of H_2O and CO_2" [Combust. Flame 247 (2023) 112498]

Ashkan Beigzadeh [a,c,*], Mohammed Alabbad [b,*], Dapeng Liu [b], Khalid Aljohani [b,d], Khaiyom Hakimov [b], Touqeer Anwar Kashif [b], Kourosh Zanganeh [a], Eric Croiset [c], Aamir Farooq [b]

[a] Natural Resources Canada (NRCan), CanmetENERGY-Ottawa (CE-O), 1 Haanel Dr., Ottawa, ON K1A 1M1, Canada
[b] Clean Combustion Research Center, Physical Sciences and Engineering Division, King Abdullah University of Science and Technology, Thuwal 23955, Saudi Arabia
[c] Department of Chemical Engineering, University of Waterloo, 200 University Avenue West, Waterloo, ON N2L 3G1, Canada
[d] Department of Mechanical Engineering, College of Engineering in Al-Kharj, Prince Sattam Bin Abdulaziz University, Al-Kharj 11942, Saudi Arabia

The Authors regret that within the abovementioned article the Affiliations were incomplete. The correct list of affiliations can be found above.

DOI of original article: https://doi.org/10.1016/j.combustflame.2022.112498.
* Corresponding authors.
E-mail addresses: ashkan.beigzadeh@NRCan-RNCan.gc.ca (A. Beigzadeh), mohammed.abbad@kaust.edu.sa (M. Alabbad).

https://doi.org/10.1016/j.combustflame.2024.113520

Available online 25 May 2024